Turbulent Reconnection after Formation of Bipolar Structures from Stratified Helical Dynamos

I. ROGACHEVSKII, N. KLEEORIN,

Ben-Gurion University of the Negev, Beer Sheva, Israel

NORDITA, KTH Royal Institute of Technology and Stockholm University, Sweden

A. BRANDENBURG, S. JABBARI, Dh. MITRA

NORDITA, KTH Royal Institute of Technology and Stockholm University,
and Department of Astronomy, Stockholm University, Sweden

Thanks to

A. Schekochihin (Oxford) and N. Loureiro (UTL, Lisboa)

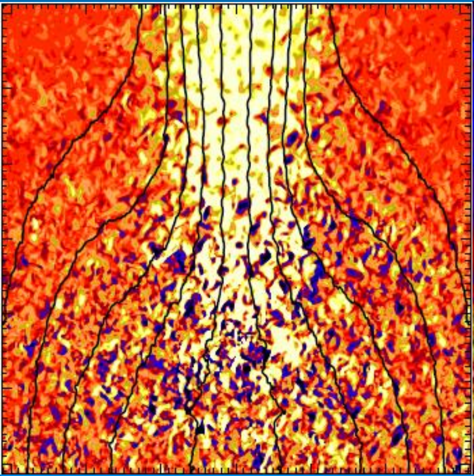

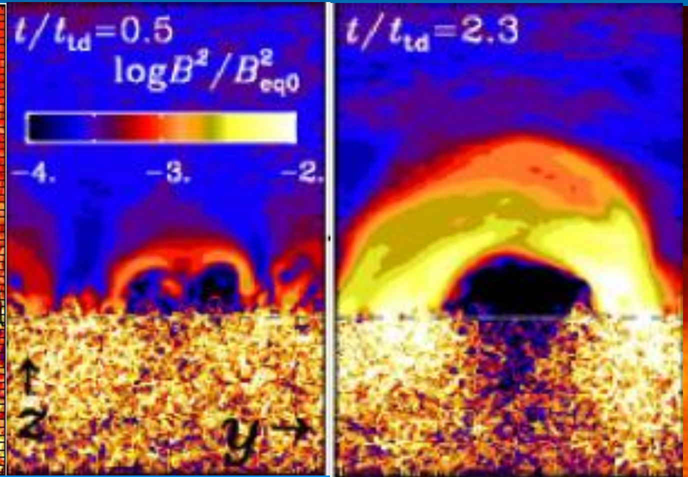

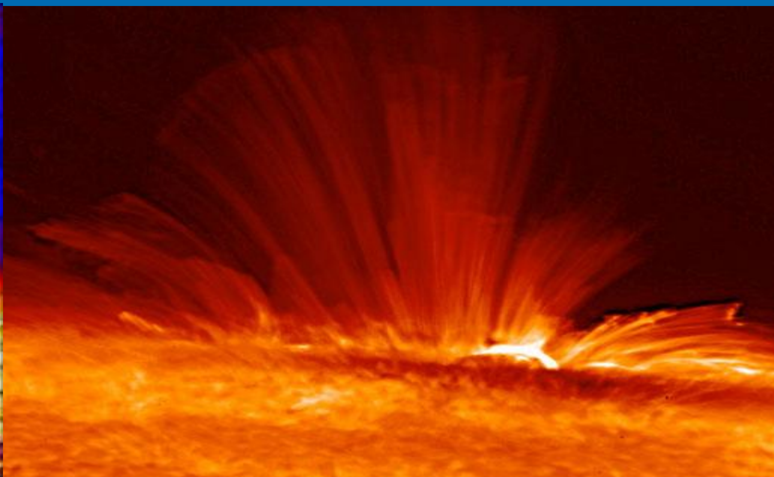

Active regions and Sunspots

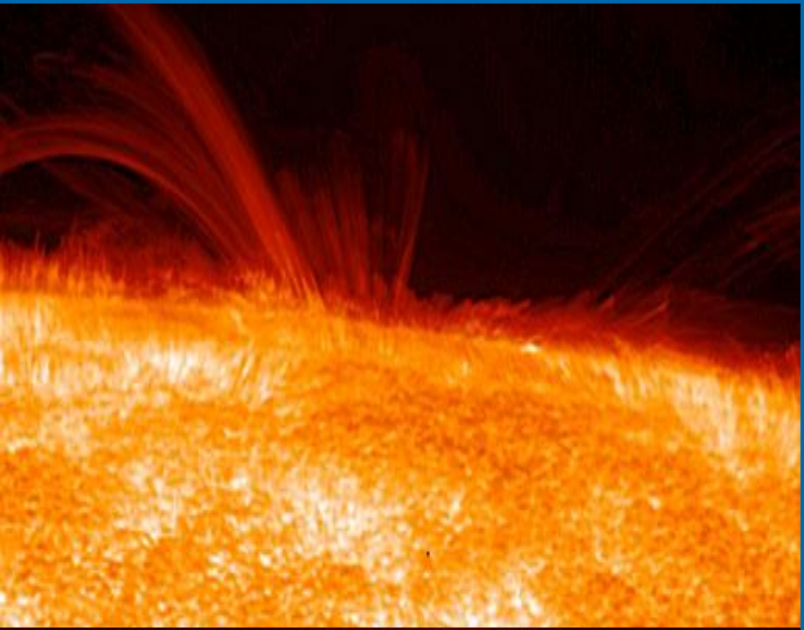

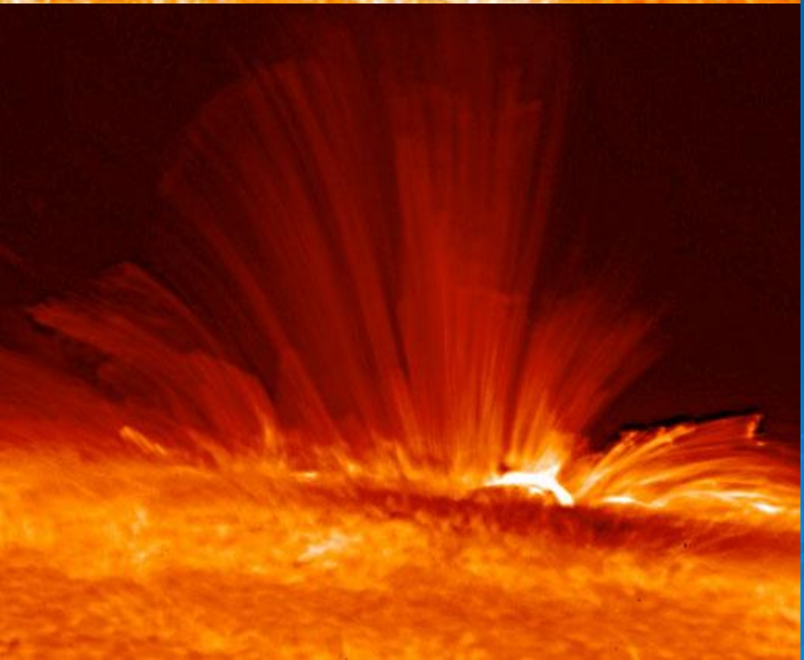

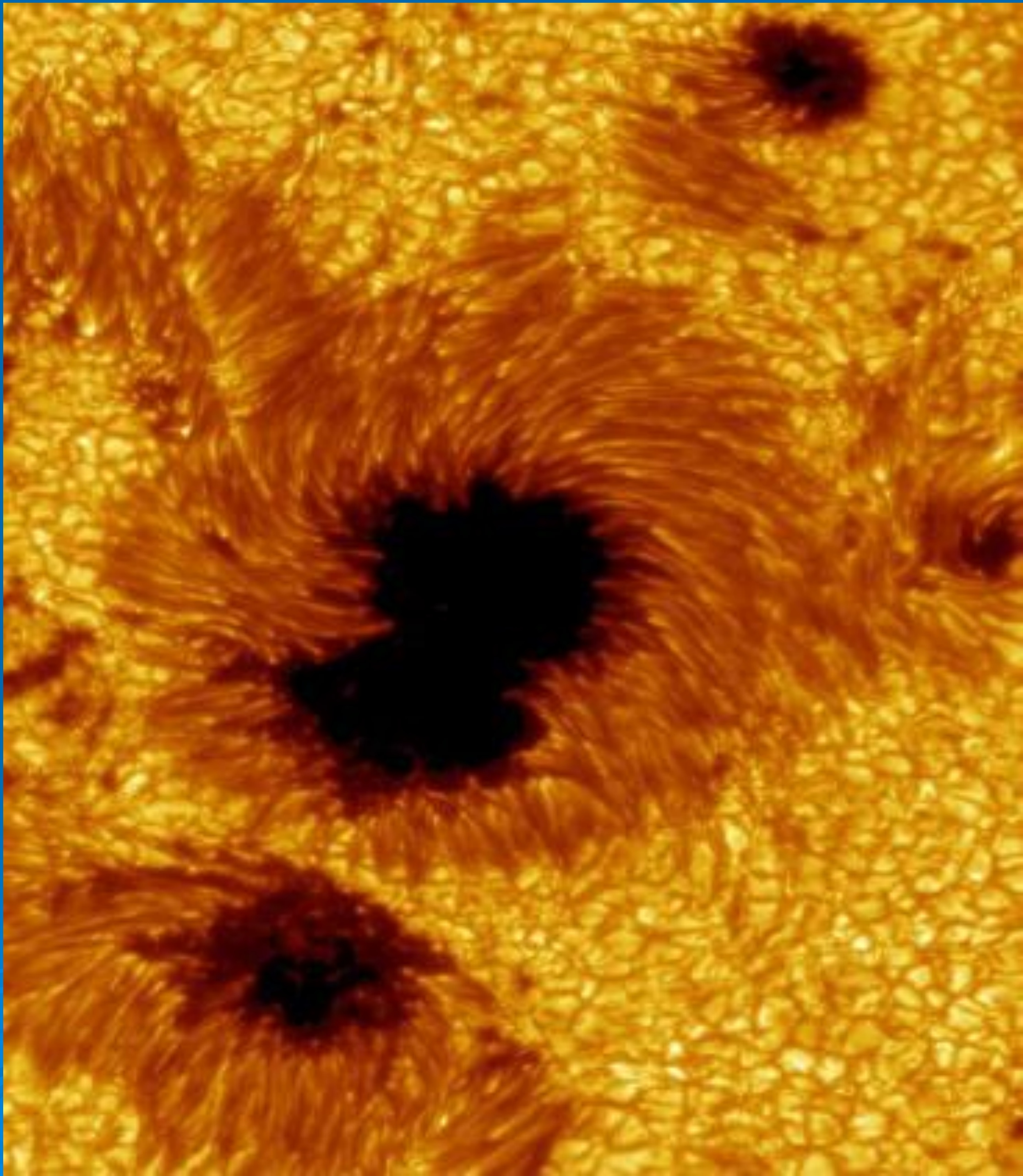

Active regions

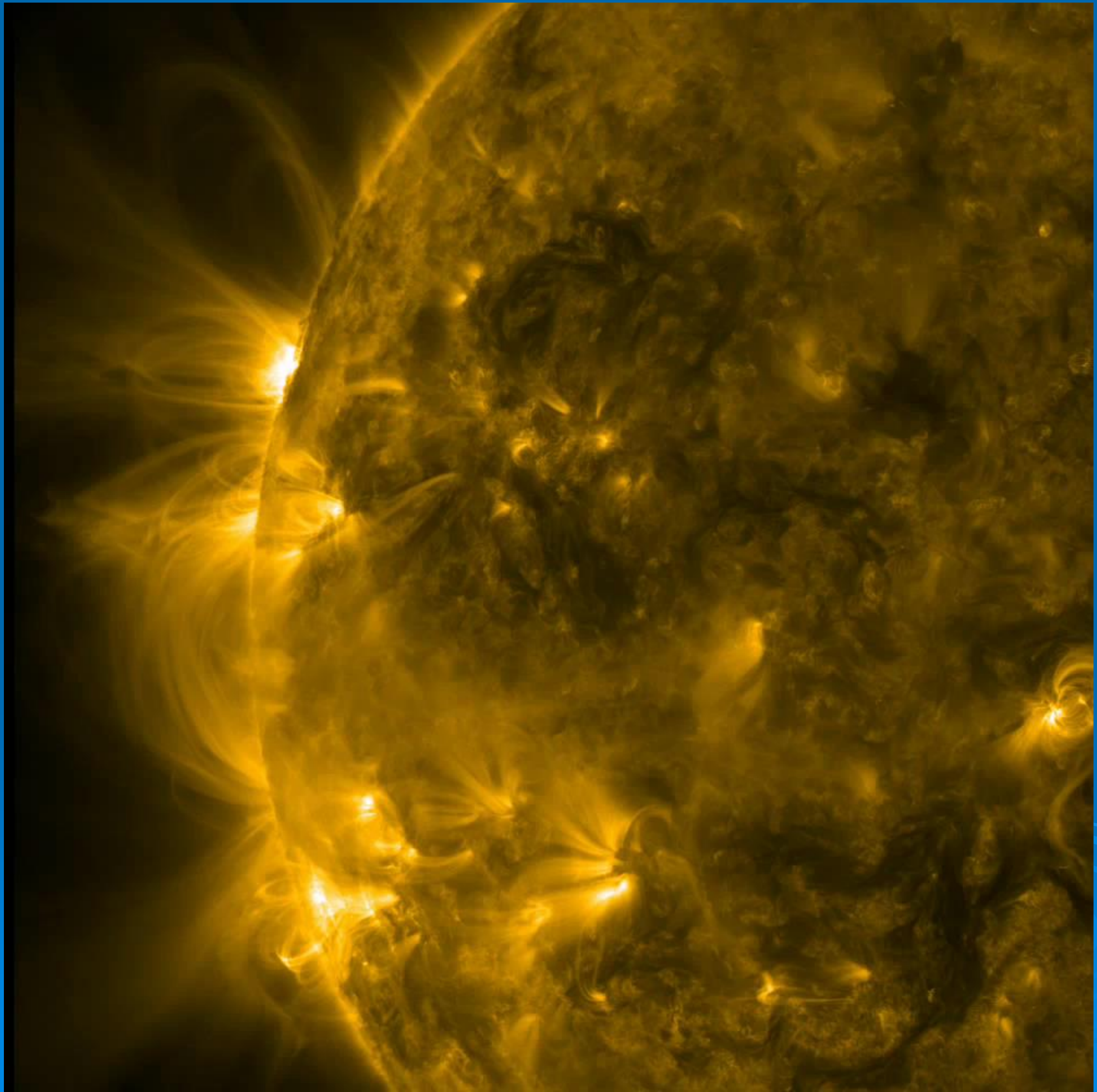

Solar convection

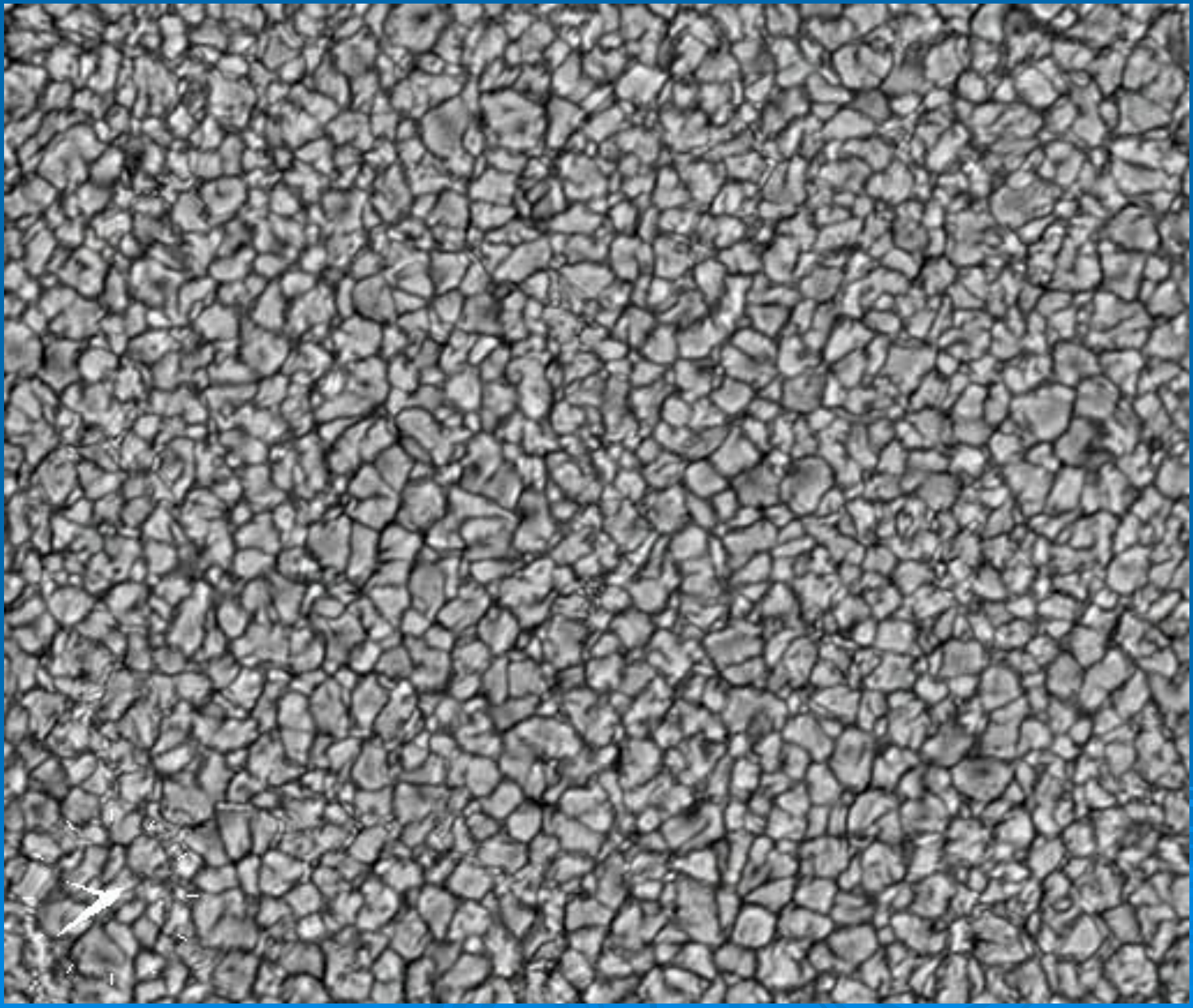

Problems

- **What is the mechanism of formation of solar magnetic structures in turbulent convection zone?**
- **Solar dynamo mechanism can generate only weak (<< 1000G) nearly uniform large-scale magnetic field.**
- **How is it possible to create strongly inhomogeneous magnetic structures from originally uniform magnetic field?**

Theories of Sunspots Formation

1. Flux-Transport Dynamo

- 1). The solar dynamo produces strong magnetic fields at the bottom of the convection zone at the tachocline region (Parker 1975; Spiegel & Weiss 1980; Spiegel & Zahn 1992, Schou et al. 1998), where there is a strong shear layer, that produces strong toroidal magnetic field.
- 2) The field becomes unstable and rises upward in form of flux tubes, which reach the surface of the sun and form bipolar structures and sunspots (Caligari et al. 1995).

Criticism:

- A) However, the field in the tachocline region should be reach $10^5 G$, which is needed for a coherent flux tube to reach the surface without strong distortion (Choudhuri & Gilman 1987; D'Silva & Choudhuri 1993).
- B) The generation of such strong coherent magnetic flux tubes has not yet been seen in self-consistent dynamo simulations (Guerrero & Käpylä 2011; Nelson et al. 2011; Fan & Fang 2014).
- C) Helioseismology also does not support a deeply rooted flux tube scenario (Kosovichev & Stenflo 2008, Stenflo & Kosovichev 2012, Howe et al. 2009; Antia & Basu 2011).

2. Negative Effective Magnetic Pressure Instability (NEMPI)

Lorentz Force and Momentum Equation

$$\mathbf{J}\times\mathbf{B} = (\boldsymbol{\nabla}\times\mathbf{B})\times\mathbf{B} = -\boldsymbol{\nabla}\frac{\mathrm{B}^2}{2}+(\mathbf{B}\cdot\boldsymbol{\nabla})\mathbf{B} = -\nabla_j\left[\frac{1}{2}\boldsymbol{B}^2\delta_{ij} - B_iB_j\right]$$

$$\frac{\partial}{\partial t}\rho\,\mathbf{U}_i = -\nabla_j\,\Pi_{ij}$$

where

$$\Pi_{ij} = \rho\,U_iU_j + \delta_{ij}\,(p+\frac{1}{2}\mathbf{B}^2) - B_iB_j - \sigma^{\nu}_{ij}(\mathbf{U}) + \ldots$$

Averaged equation: $\mathbf{U} = \bar{\mathbf{U}} + \mathbf{u}$, $\mathbf{B} = \bar{\mathbf{B}} + \mathbf{b}$

$$\frac{\partial}{\partial t}\bar{\rho}\,\bar{\mathbf{U}}_i = -\nabla_j\,\bar{\Pi}_{ij}$$

where

$$\bar{\Pi}_{ij} = \bar{\rho}\,\bar{U}_i\bar{U}_j + \delta_{ij}\,(\bar{p}+\frac{1}{2}\bar{\mathbf{B}}^2) - \bar{B}_i\bar{B}_j - \bar{\sigma}^{\nu}_{ij}(\bar{\mathbf{U}}) + \frac{1}{2}\langle \mathbf{b}^2\rangle\,\delta_{ij} - \langle b_ib_j\rangle + \bar{\rho}\langle u_iu_j\rangle + \ldots$$

DNS: 3D Stratified Forced Turbulence

Effective Mean Magnetic Pressure

(sum of turbulent and non-turbulent contributions)

$$\mathrm{J}\times\mathrm{B} = (\nabla\times\mathrm{B})\times\mathrm{B} = -\nabla\frac{\mathrm{B}^2}{2} + (\mathrm{B}\cdot\nabla)\mathrm{B} = -\nabla_j\left[\frac{1}{2}B^2\delta_{ij} - B_iB_j\right]$$

$$\mathcal{P}_{\rm eff}(\beta) = \tfrac{1}{2}[1 - q_{\rm p}(\beta)]\,\beta^2 \quad \text{versus} \quad \beta \equiv |\overline{\boldsymbol{B}}|/B_{\rm eq}$$

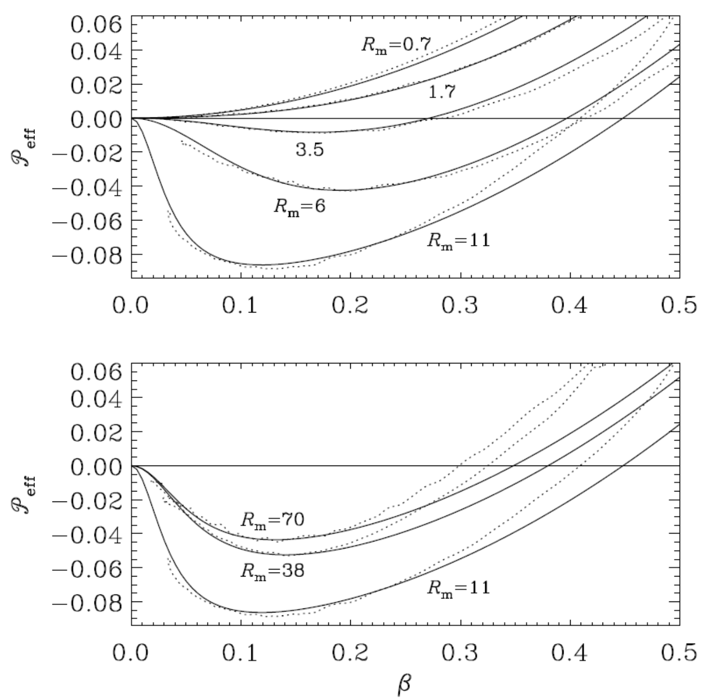

Figure 7. Normalized effective magnetic pressure, $\mathcal{P}_{\rm eff}(\beta)$, for low (upper panel) and higher (lower panel) values of Re_M. The solid lines represent the fits to the data shown as dotted lines.

$$\mathrm{B} = \bar{\mathrm{B}} + \mathrm{b}$$

$$\mathcal{P}_{\rm eff} = \frac{1}{2}(1 - q_p)\frac{\bar{\mathrm{B}}^2}{\mathrm{B}_{\rm eq}^2}$$

Effective magnetic pressure for Rm < 1 is positive, and for Rm > 1, it can be negative.

Quasi-linear theory works only for

$$\mathrm{Rm} \ll 1$$

Equation of State for Isotropic Turbulence

N. Kleeorin, I. Rogachevskii and A. Ruzmaikin,
Sov. Astron. Lett. 15, 274-277 (1989); Sov. Phys. JETP 70, 878-883 (1990)

N. Kleeorin and I. Rogachevskii, *Phys. Rev. E 50, 2716-2730 (1994)*

I. Rogachevskii and N. Kleeorin, *Phys. Rev. E 76, 056307 (2007)*

The total turbulent pressure is reduced when magnetic fluctuations are generated

The equation of state for an isotropic turbulence

$$p_T = \frac{1}{3} W_m + \frac{2}{3} W_k \ ,$$

where p_T is the total (hydrodynamic plus magnetic) turbulent pressure,

$W_m = \langle \mathbf{b}^2 \rangle / 2\mu$ is the energy density of the magnetic fluctuations,

$W_k = \rho_0 \langle \mathbf{u}^2 \rangle / 2$ is the kinetic energy density.

Strong reduction of Turbulent Pressure

Magnetic contribution to pressure & energy different!

$$U_iU_j - B_iB_j + \tfrac{1}{2}\delta_{ij}\mathbf{B}^2$$
$$\approx \tfrac{1}{3}\delta_{ij}\left(\mathbf{U}^2 + \tfrac{1}{2}\mathbf{B}^2\right)$$
$$\approx \tfrac{1}{3}\delta_{ij}\left(\underbrace{\mathbf{U}^2 + \mathbf{B}^2}_{\approx const} - \tfrac{1}{2}\mathbf{B}^2\right)$$

Can lead to reversed mean-field buoyancy in *stratified* system

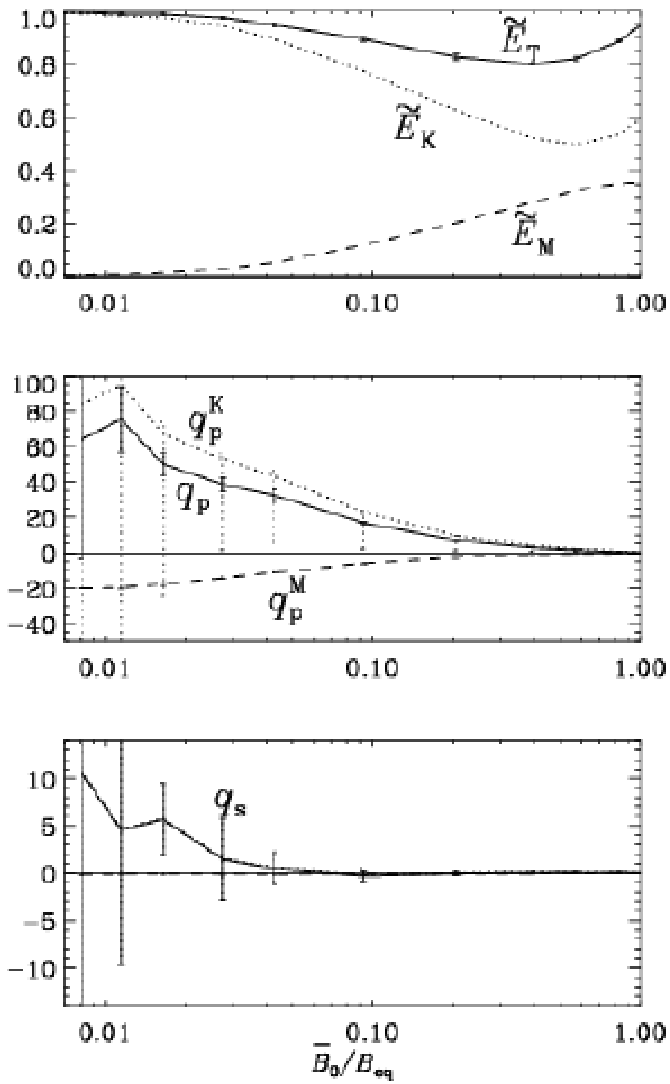

Strong reduction of Turbulent Pressure

Combining the equations:

$$p_T = \frac{1}{3}W_m + \frac{2}{3}W_k = \frac{2}{3}(W_k + W_m) - \frac{1}{3}\mathrm{W_m}\,, \qquad \mathrm{W_k} + \mathrm{W_m} = \mathrm{const}\,,$$

we can express the change of turbulent pressure δp_T in terms of the change of the magnetic energy density δW_m

$$\delta \mathrm{p_T} = -\frac{1}{3}\delta \mathrm{W_m}$$

Therefore, the turbulent pressure is reduced when magnetic fluctuations are generated (i.e., $\delta \mathrm{W_m} > 0$).

DNS: The Result is Robust

$$\mathcal{P}_{\rm eff} = \frac{1}{2}(1-q_p)\frac{\bar{\rm B}^2}{{\rm B}_{\rm eq}^2}$$

Effect does not exist only below $\mathrm{Rm} = 1$

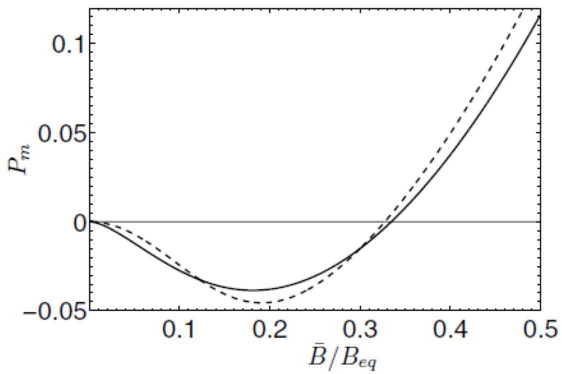

Fig. 3 The effective mean magnetic pressure $P_m(\overline{B}) = (1 - q_{\rm p})\overline{B}^2/\overline{B}_{\rm p}^2$ determined by Rogachevskii & Kleeorin (2007) – solid line, and by the model described by Eq. (26) – dashed line ($\overline{B}_{\rm p} = 0.21\,c_{\rm s0}\rho_0^{1/2}$ and $q_{\rm p0} = 4$).

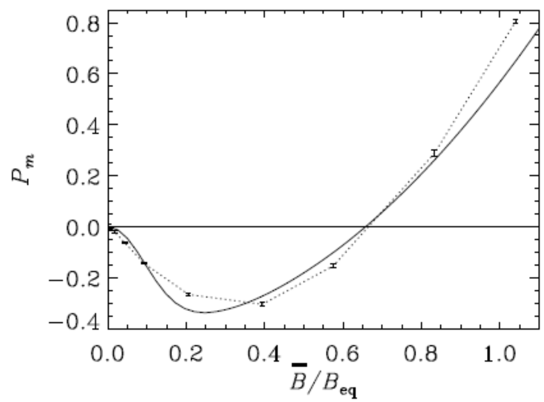

Fig. 4 Same as Fig. 3, but from simulation (dotted line). The solid line shows a fit [Eq. (26)] with $\overline{B}_{\rm p} = 0.022\,c_{\rm s0}\rho_0^{1/2}$ (corresponding to $\overline{B}_{\rm p}/B_{\rm eq} = 0.18$) and $q_{\rm p0} = 21$.

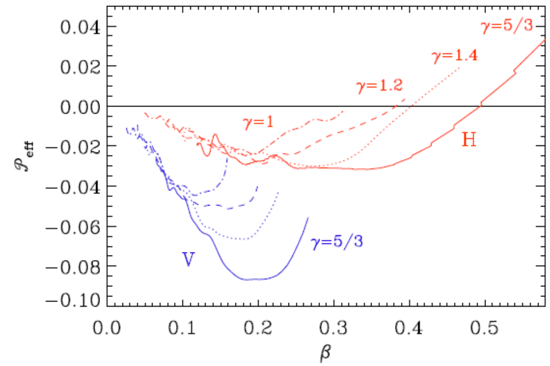

Fig. 7. Effective magnetic pressure obtained from DNS in a polytropic layer with different γ for horizontal (H, red curves) and vertical (V, blue curves) mean magnetic fields.

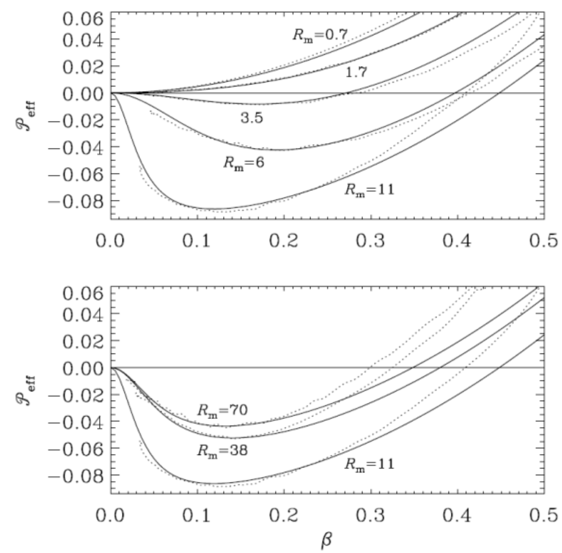

Figure 7. Normalized effective magnetic pressure, $\mathcal{P}_{\rm eff}(\beta)$, for low (upper panel) and higher (lower panel) values of Re_M. The solid lines represent the fits to the data shown as dotted lines.

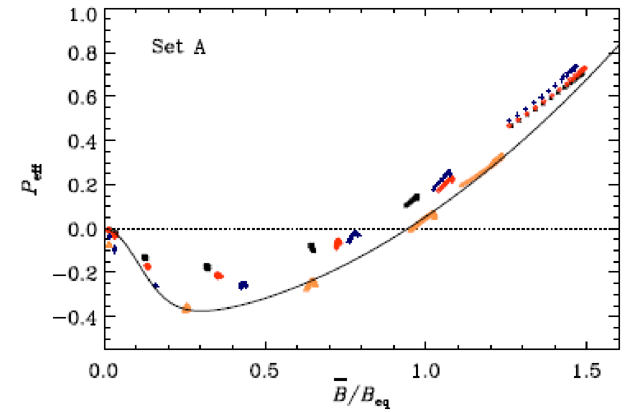

Figure 2. Effective magnetic pressure as a function of the mean magnetic field from weakly stratified Runs A1–A29 with an imposed horizontal field $\boldsymbol{B}_0 = B_0\hat{\boldsymbol{x}}$. The black stars, red diamonds, blue crosses, and yellow triangles denote simulations with Rm $\approx$ 10, 20, 50, and 70, respectively. We omit points near the boundaries at $z/d < 0.35$ and $z/d > 0.65$. The dashed and dotted lines correspond to approximate fits determined by Eq. (30), with $q_{\rm p0} = 35$ and $B_{\rm p} = 0.2B_{\rm eq}$, respectively.

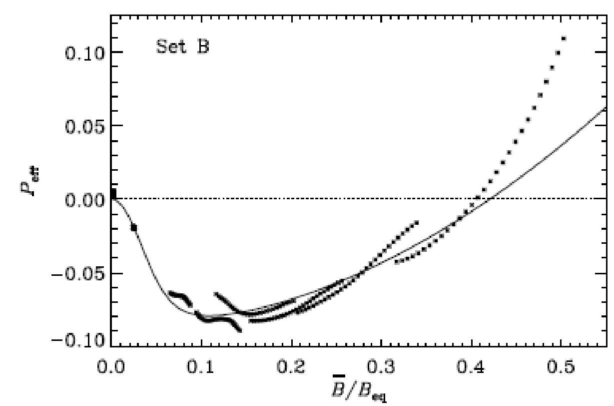

Figure 3. Same as Figure 2 but for Runs B1–B8 for Rm = 40–50. The solid line corresponds to a fit with $q_{\rm p0} = 70$ and $B_{\rm p} = 0.063B_{\rm eq}$

Large-Scale MHD-Instability (NEMPI)

A. Brandenburg, K. Kemel, N. Kleeorin, Dh. Mitra, and I. Rogachevskii,
Astrophys. J. Lett. 740, L50 (2011); Solar Phys. 280, 321-333 (2012).

Slow growth

$$\lambda = \frac{v_A}{H_\rho}\left(-2\frac{d\mathcal{P}_{\rm eff}}{d\beta^2}\right)^{1/2}\frac{k_x}{k}.$$

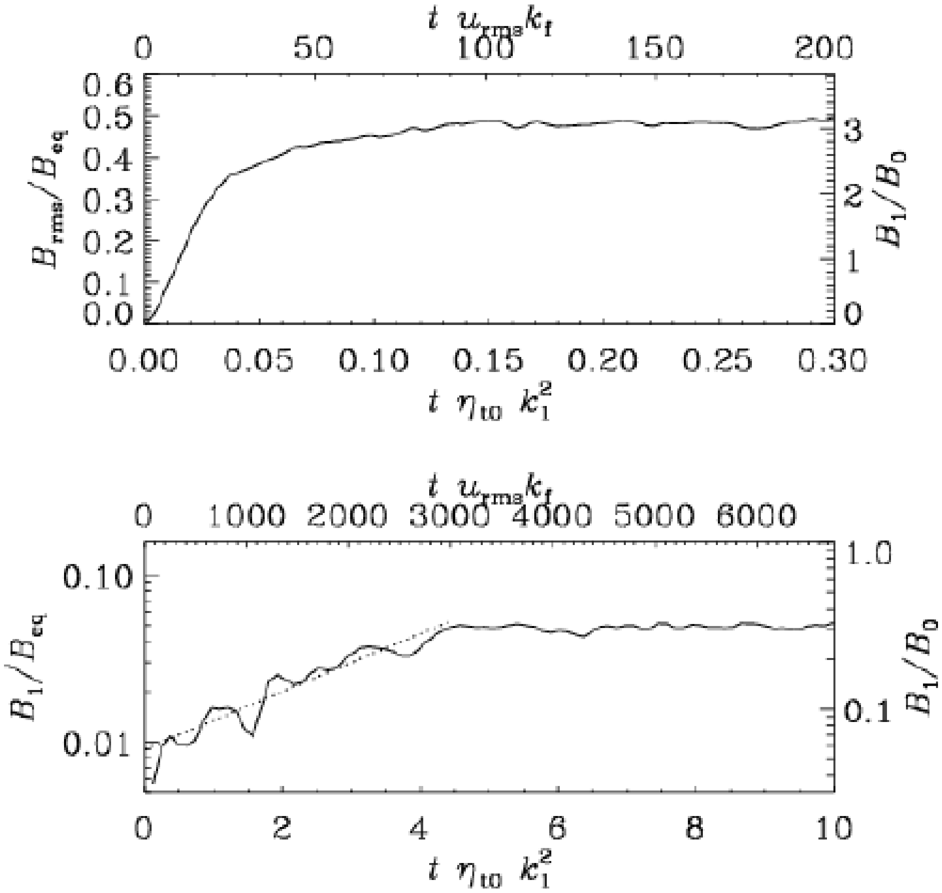

- Several thousand turnover times
- Or ½ a turbulent diffusive time
- Exponential growth → linear instability of an already turbulent state

NEMPI in DNS: 3D Forced Turbulence (Vertical Imposed Weak Magnetic Field)

All simulations are performed with the PENCIL CODE, that uses sixth-order explicit finite differences in space and a third-order accurate time stepping method.

$$\rho \frac{\mathrm{D}\boldsymbol{U}}{\mathrm{D}t} = -c_\mathrm{s}^2 \boldsymbol{\nabla} \rho + \boldsymbol{J} \times \boldsymbol{B} + \rho(\boldsymbol{f} + \boldsymbol{g}) + \boldsymbol{\nabla} \cdot (2\nu\rho\mathbf{S}),$$

$$\frac{\partial \boldsymbol{A}}{\partial t} = \boldsymbol{U} \times \boldsymbol{B} + \eta \nabla^2 \boldsymbol{A},$$

$$\frac{\partial \rho}{\partial t} = -\boldsymbol{\nabla} \cdot \rho \boldsymbol{U},$$

$$\boldsymbol{B} = \boldsymbol{B}_0 + \boldsymbol{\nabla} \times \boldsymbol{A}$$

$$\mathrm{Rm} = \frac{u_{rms}}{\eta\, k_f} = 18, 40, 95$$

$$\mathrm{Pm} = \frac{\nu}{\eta} = \frac{1}{2}$$

$$k_f = 30\, k_1;$$

$$\frac{\rho_{bot}}{\rho_{top}} = 535;$$

BOUNDARY CONDITIONS at the top and bottom:

$$U_z = 0, \quad \nabla_z U_x = \nabla_z U_y = 0$$

$$B_x = B_y = 0,$$

BOUNDARY CONDITIONS:

1). The horizontal boundaries are periodic.

2). For the velocity we apply impenetrable, stress-free conditions.

3). For the magnetic field we use vertical field boundary conditions.

Formation of Magnetic Spots in DNS

(Vertical Imposed Weak Magnetic Field)

PENCIL CODE

$$256^3; 512^3; 1024^3$$

$k_f = 30\, k_1;$

$\mathrm{Rm} = \frac{u_{rms}}{\eta\, k_f} = 18; 40; 95$

$\mathrm{Pm} = \frac{\nu}{\eta} = \frac{1}{2}$

$\frac{\rho_{bot}}{\rho_{top}} = 535;$

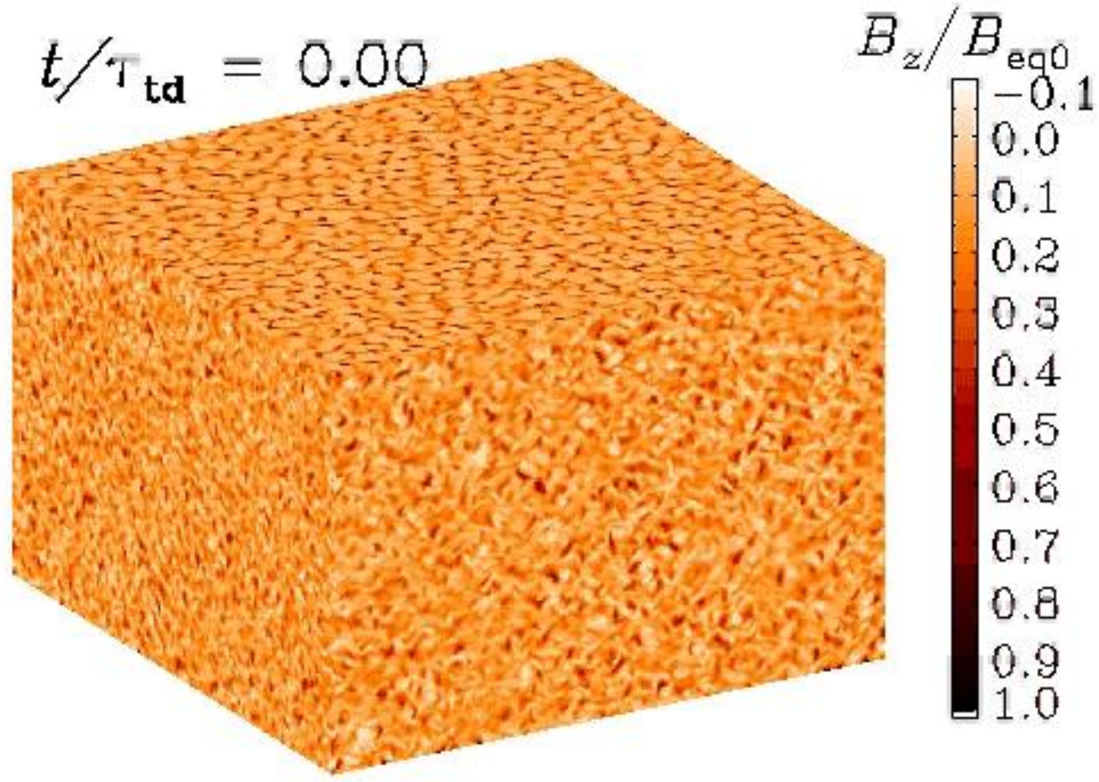

BOUNDARY CONDITIONS at the top and bottom:

1. stress-free conditions

$\nabla_z U_x = \nabla_z U_y = 0$

$U_z = 0,$

2. vertical field

$B_x = B_y = 0,$

A. Brandenburg, N. Kleeorin and I. Rogachevskii, Astrophys. J. Lett., 776, L23 (2013)

Formation and Destruction of Bipolar Magnetic Structures

J. Warnecke, I.R. Losada, A. Brandenburg, N. Kleeorin and I. Rogachevskii,

Astrophys. J. Lett., 777, L37 (2013); Astron. Astrophys., submitted (2015)

Imposed horizontal field.

$$k_f = 30\, k_1;$$

BOUNDARY CONDITIONS at the top and bottom:

$$U_z = 0, \;\; \nabla_z U_x = \nabla_z U_y = 0$$

But

$$z = -\pi:$$

$$B_z = 0, \;\; \nabla_z B_x = \nabla_z B_y = 0$$

$$z = 2\pi:$$

$$B_x = B_y = 0.$$

Re=40, $\mathrm{Pr}_M = 0.06 - 1$

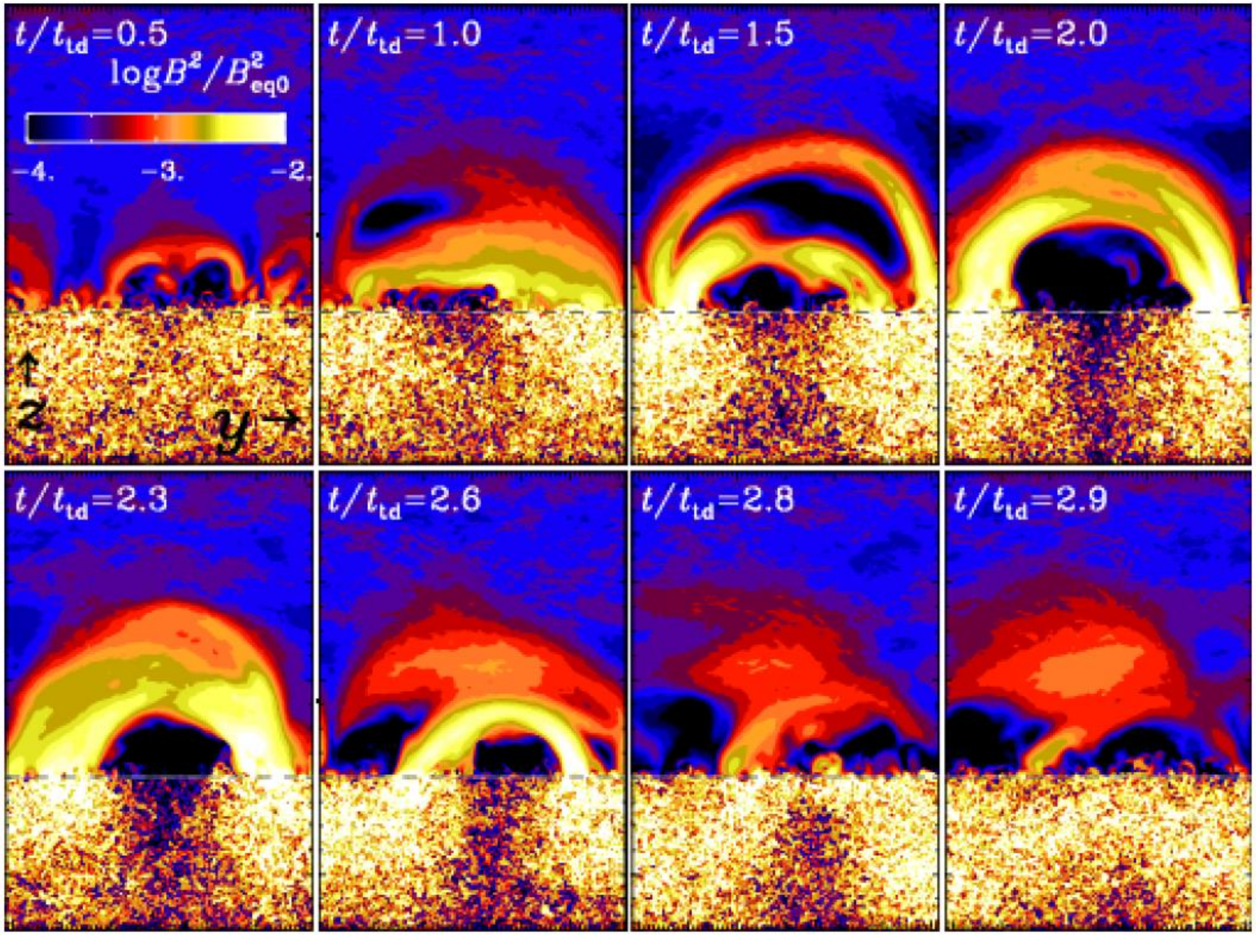

FIG. 5.— Time series of B^2/B^2_{eq0} in a vertical cut through the bipolar region at $x = 0$. Note the y axis is shifted the see the formation of the loop.

Formation and Destruction of Bipolar Magnetic Structures

J. Warnecke, I.R. Losada, A. Brandenburg, N. Kleeorin and I. Rogachevskii,
Astrophys. J. Lett., 777, L37 (2013); Astron. Astrophys., submitted (1015).

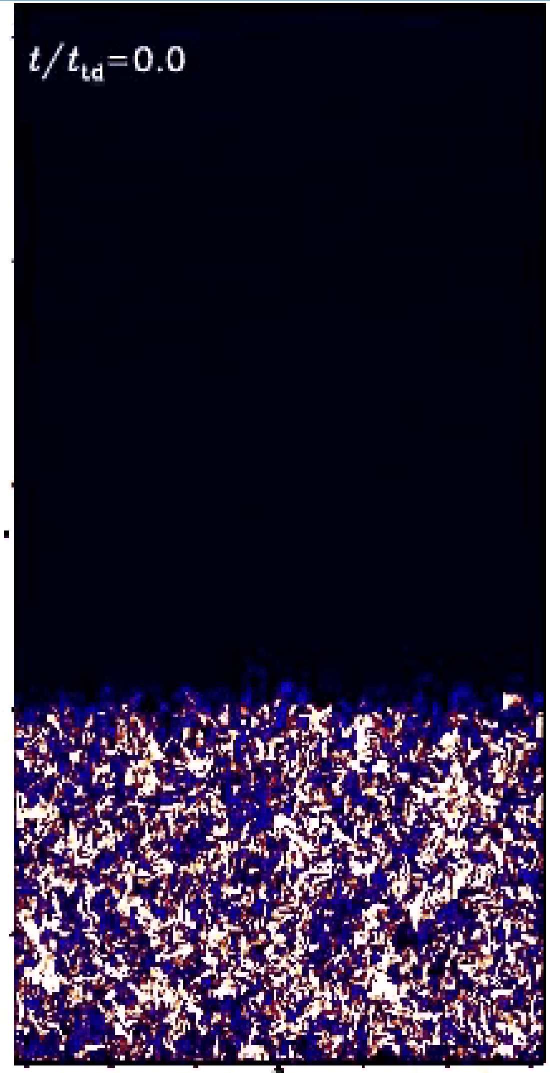

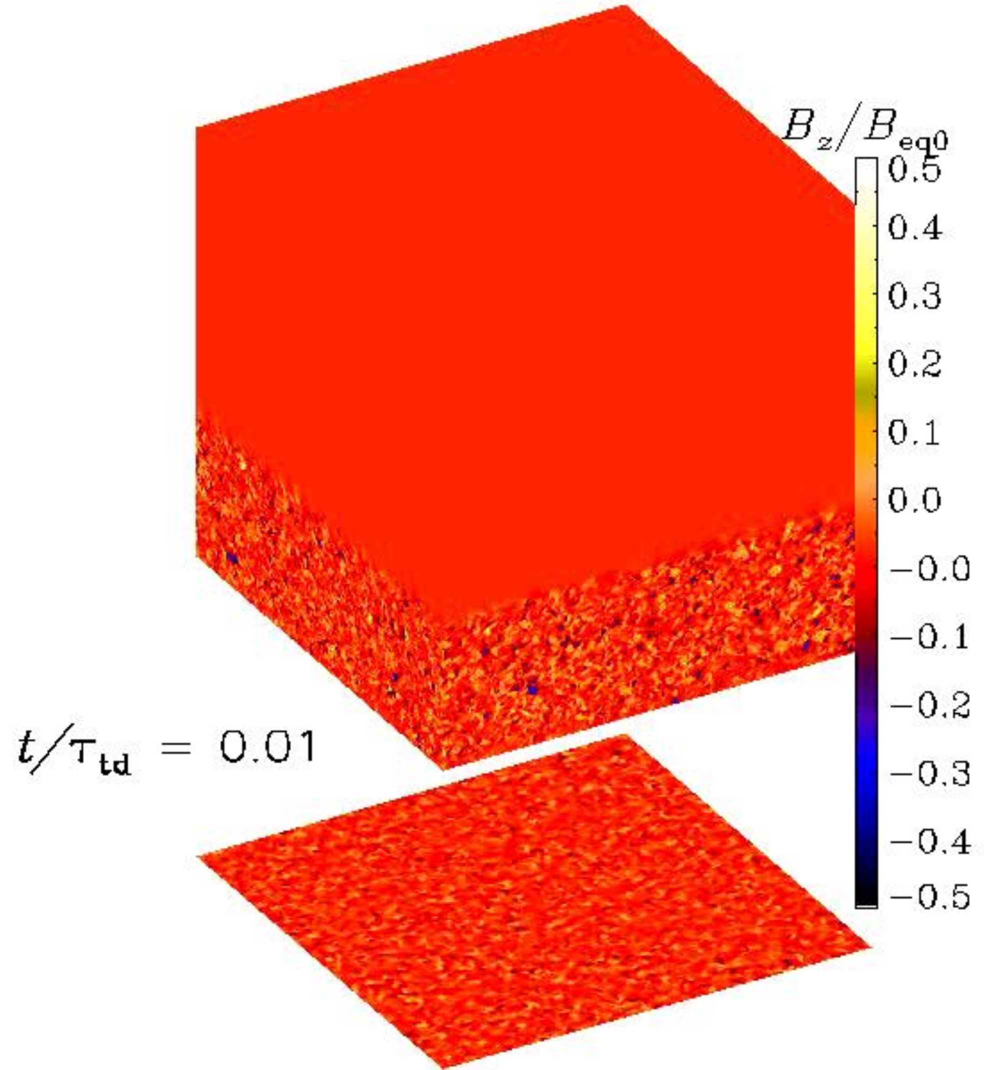

Formation and Destruction of Bipolar Magnetic Structures

J. Warnecke, I.R. Losada, A. Brandenburg, N. Kleeorin and I. Rogachevskii,
Astrophys. J. Lett., 777, L37 (2013); Astron. Astrophys., submitted (2015)

Imposed horizontal field.

$k_f = 30\,k_1;$

BOUNDARY CONDITIONS at the top and bottom:

$U_z = 0, \ \ \nabla_z U_x = \nabla_z U_y = 0$

But

$z = -\pi:$

$B_z = 0, \ \ \nabla_z B_x = \nabla_z B_y = 0$

$z = 2\pi:$

$B_x = B_y = 0.$

Re=40, $\mathrm{Pr}_M = 0.06 - 1$

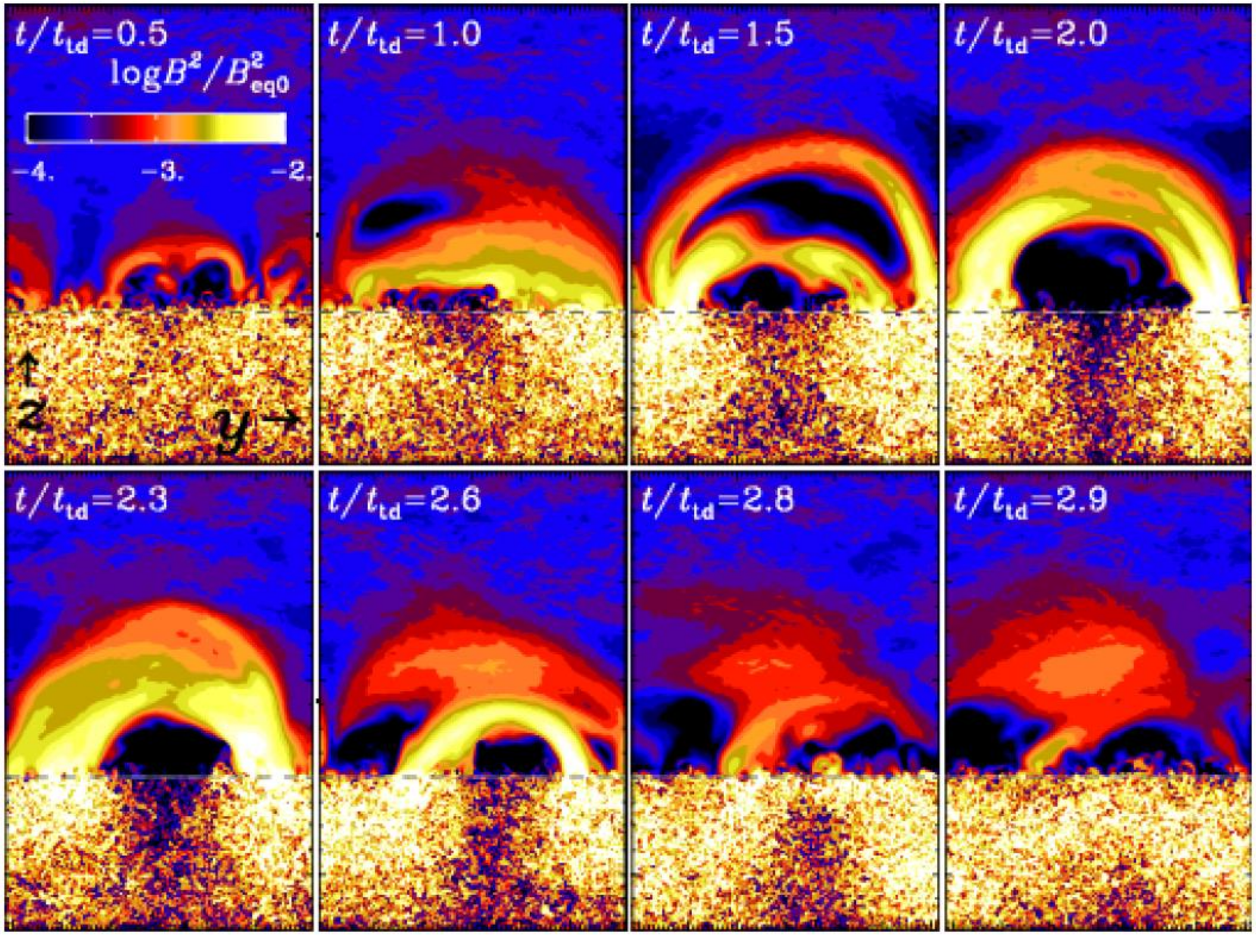

FIG. 5.— Time series of B^2/B^2_{eq0} in a vertical cut through the bipolar region at $x = 0$. Note the y axis is shifted the see the formation of the loop.

Magnetic Structures

J. Warnecke, I.R. Losada, A. Brandenburg, N. Kleeorin and I. Rogachevskii,
Astrophys. J. Lett., 777, L37 (2013), Astron. Astrophys., submitted (2015).

Simulations

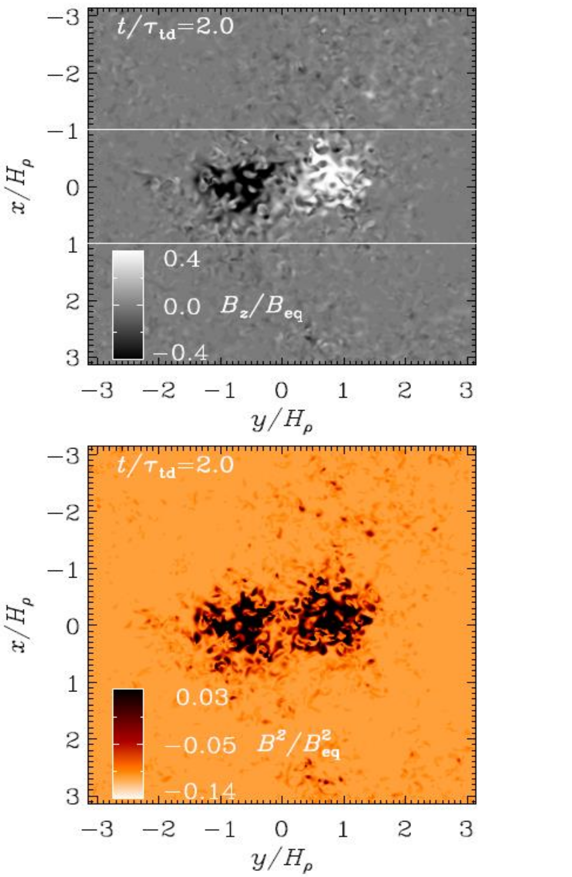

FIG. 1.— *Upper panel:* normalized vertical magnetic field B_z/B_{eq} of the bipolar region at the surface ($z = 0$) of the simulation domain. The white lines delineate the area shown in Figure 3. *Lower panel:* normalized magnetic energy B^2/B_{eq}^2 of the two regions relative to the rest of the surface. Note that we clip both color tables to increase the visualization of the structure. The field strength reaches around $B_z/B_{eq} = 1.4$.

Sunspots

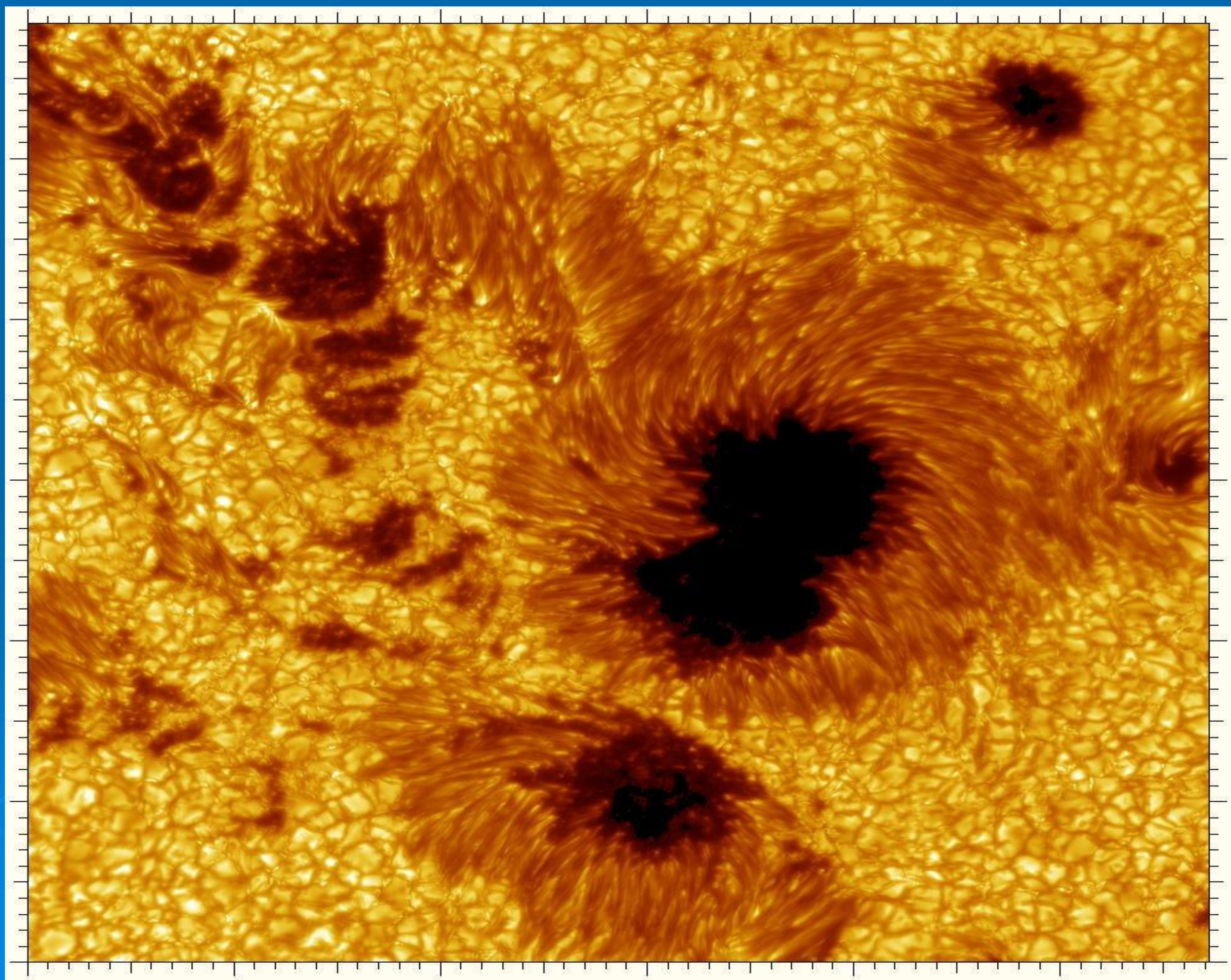

DNS in Two Forced Regions: Dynamo+NEMPI

Dh. Mitra, A. Brandenburg, N. Kleeorin and I. Rogachevskii, MNRAS 445, 716 (2014).

All simulations are performed with the PENCIL CODE, that uses sixth-order explicit finite differences in space and a third-order accurate time stepping method.

$$\rho\frac{\mathrm{D}\boldsymbol{U}}{\mathrm{D}t} = -c_{\mathrm{s}}^2\boldsymbol{\nabla}\rho + \boldsymbol{J}\times\boldsymbol{B} + \rho(\boldsymbol{f}+\boldsymbol{g}) + \boldsymbol{\nabla}\cdot(2\nu\rho\mathbf{S}),$$

$$\frac{\partial \boldsymbol{A}}{\partial t} = \boldsymbol{U}\times\boldsymbol{B} + \eta\nabla^2\boldsymbol{A},$$

$$\frac{\partial\rho}{\partial t} = -\boldsymbol{\nabla}\cdot\rho\boldsymbol{U},$$

Run	z_0	$\sigma_{\max}$	Re_{M}	$\tilde{k}_{\mathrm{f}}$	$\tilde{\lambda}$	τ_{to}	τ_{td}
A	2	1	17	30	0.041	0.33	900
B	−1	1	17	30	0.042	0.33	900
B/2	−1	1	17	30	0.036	0.33	900
C	−2	1	17	30	0.045	0.33	900
D	−2	1	17	60	0.043	0.17	1800
E	−2	1	170	30	0.022	0.33	900
0-02	0	0.2	17	30	0.0043	0.33	900
0-1	0	1	17	30	0.043	0.33	900

$$\frac{\rho_{bot}}{\rho_{top}} = 535; \quad \mathrm{Pm} = \frac{\nu}{\eta} = \frac{1}{2}$$

$256^3; 512^3;$

FORCING:

1). White-in-time random forcing with the fractional helicity:

2). Helical forcing: $-\pi < z < z_0$ (bottom layer);

3). Non-helical forcing: $z_0 < z < \pi$ (upper layer).

$$\sigma(z-z_0) = \frac{\sigma_{\max}}{2}\left[1-\mathrm{erf}\left(\frac{z-z_0}{w_{\mathrm{f}}}\right)\right]$$

$$\mathrm{Re} \equiv u_{\mathrm{rms}}/\nu k_{\mathrm{f}}, \qquad w_f = 0.08L_z$$

BOUNDARY CONDITIONS:

1).The horizontal boundaries are periodic.

2). For the velocity we apply impenetrable, stress-free conditions.

3). For the magnetic field we use a) vertical field boundary conditions for z=L (at the top);

b) perfect conductor for z=0 (at the bottom) .

➢Dh. Mitra, A. Brandenburg, N. Kleeorin and I. Rogachevskii, **MNRAS 445, 716 (2014).**

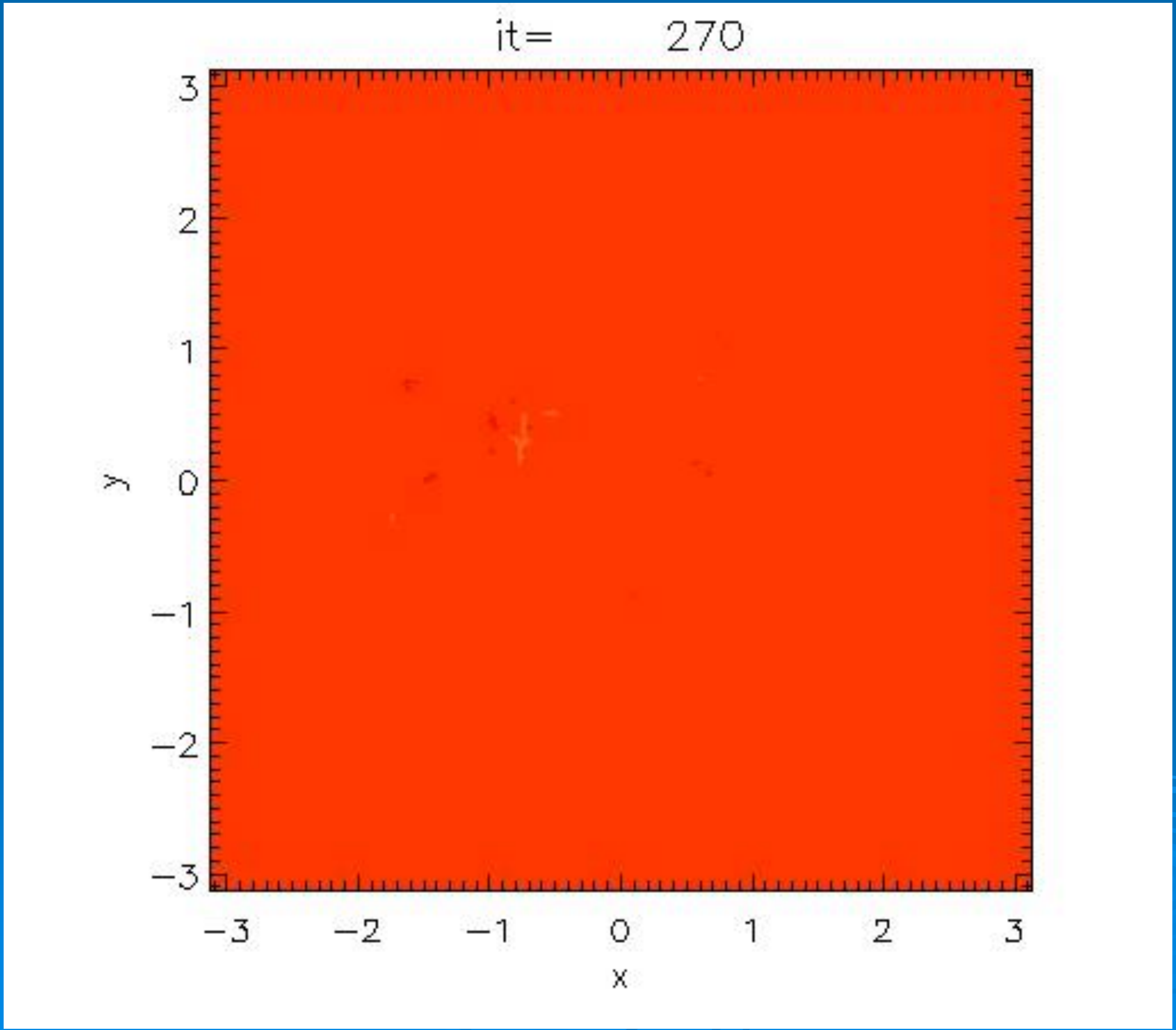

DNS in Two Forced Regions: Dynamo+NEMPI

- **Dh. Mitra, A. Brandenburg, N. Kleeorin and I. Rogachevskii,** **MNRAS 445, 716 (2014).**

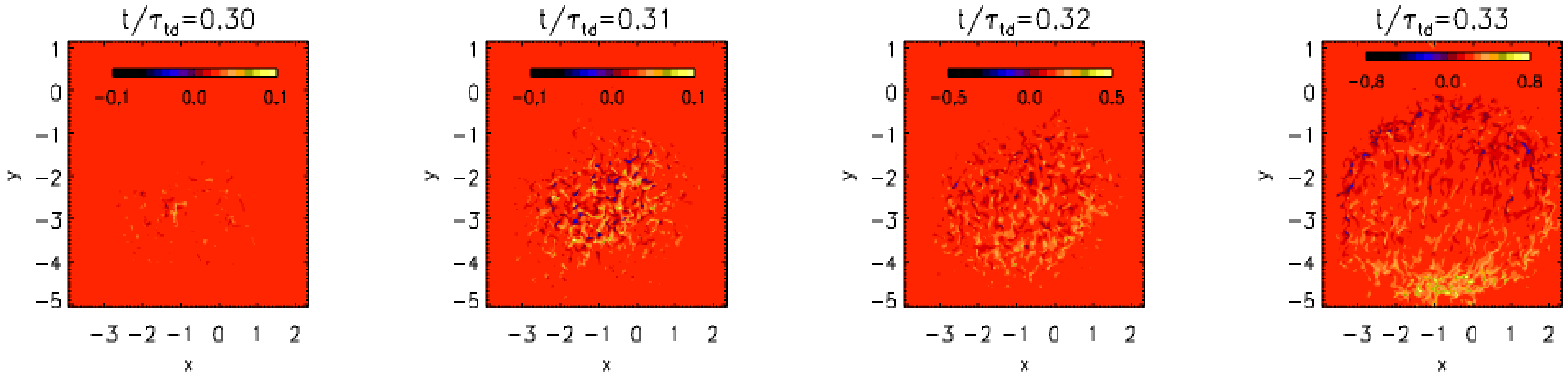

Figure 2. Vertical magnetic field at the top surface at different times (from $t/\tau_{\rm td} = 0.30$ to 0.33) from Run B. The magnetic field is normalized by $B_{\rm eq}^0$.

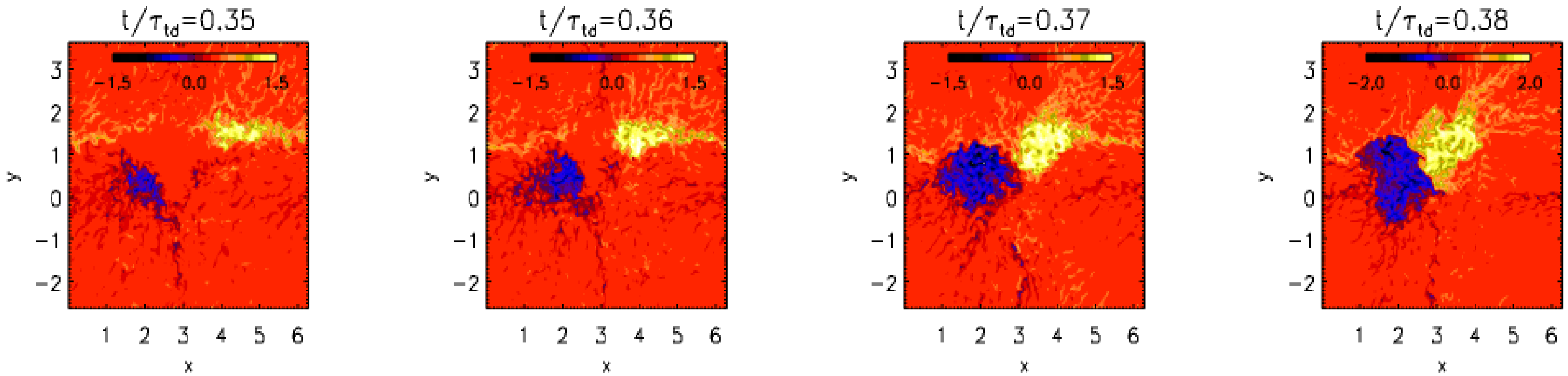

Figure 3. Same as Fig. 2, but at later times (from $t/\tau_{\rm td} = 0.35$ to 0.38) and the frame is re-centered, as illustrated in Fig. 4 below.

DNS in Two Forced Regions: Dynamo+NEMPI

➢ **Dh. Mitra, A. Brandenburg, N. Kleeorin and I. Rogachevskii, MNRAS 445, 716 (2014).**

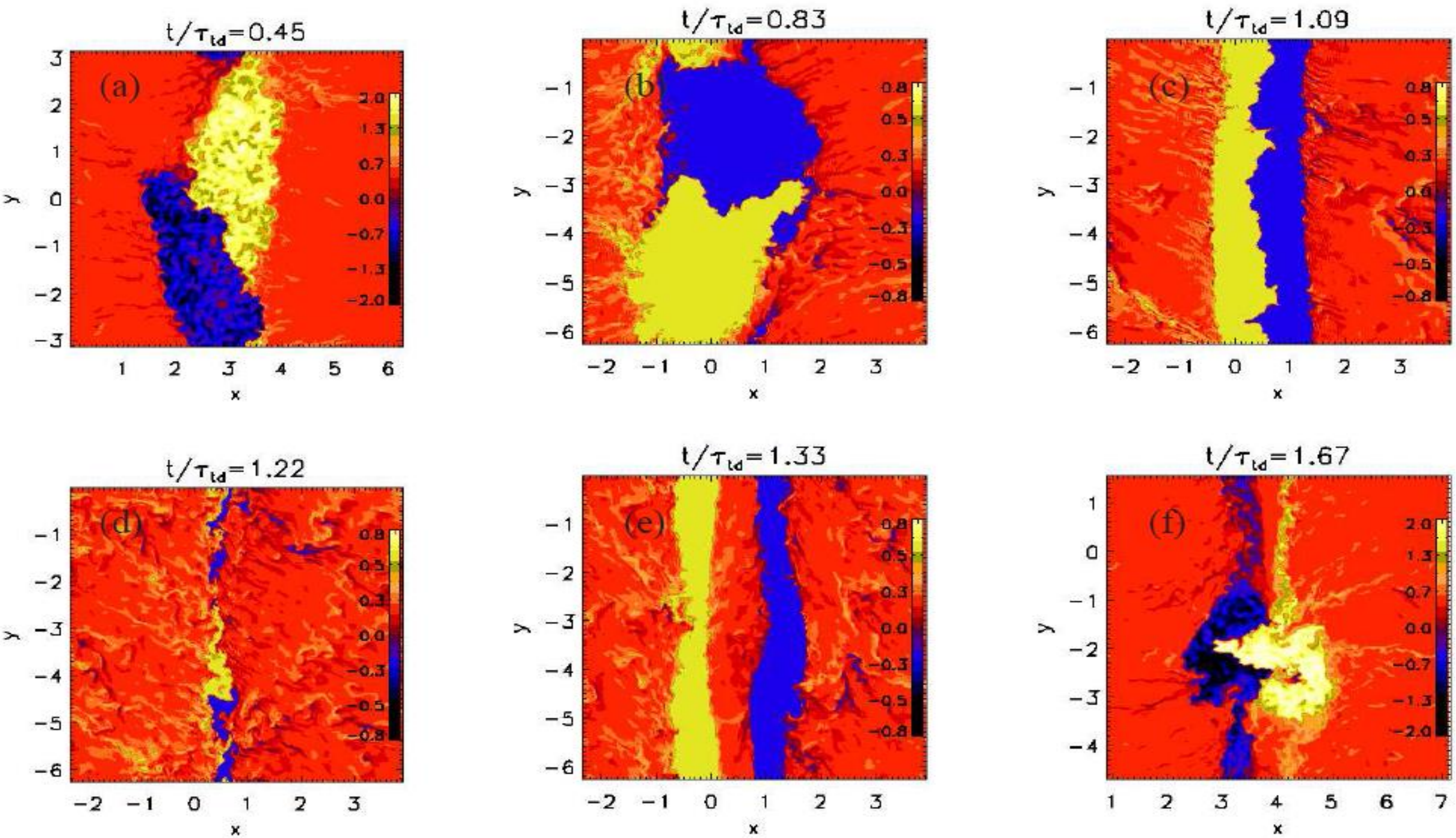

Figure 5. Evolution of the vertical magnetic field at the top surface. Snapshots at different times (from $t/\tau_{\rm td} = 0.45$ to $t/\tau_{\rm td} = 1.67$) are plotted.

DNS in Two Forced Regions: Dynamo+NEMPI

- **Dh. Mitra, A. Brandenburg, N. Kleeorin and I. Rogachevskii,** **MNRAS 445, 716 (2014).**

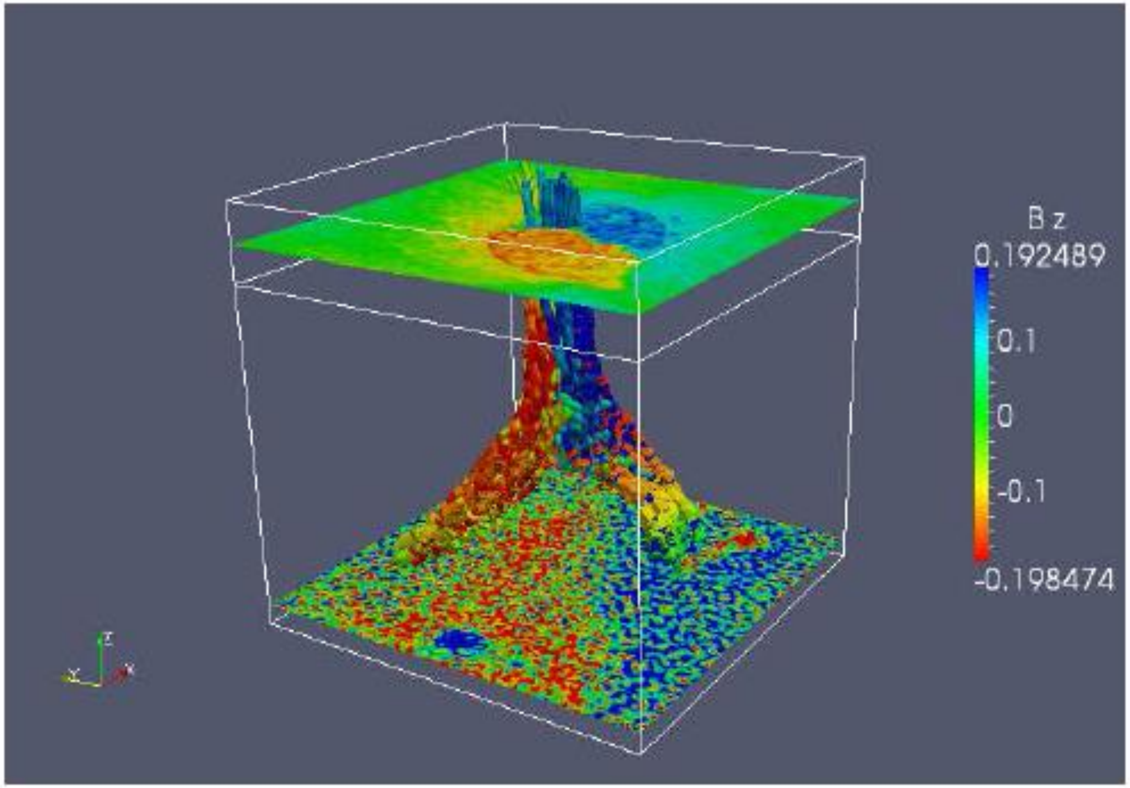

Figure 8. Magnetic field structure for Run A at time $t/\tau_{\rm td} \approx 1.2$. The z component of the magnetic field, B_z is plotted at $z/H_\rho = 3.$. The height up to which dynamo operates, $z_0/H_\rho = 2$, is also shown as a frame. Here magnetic field, B_z is not normalized, but in units of $\sqrt{\langle\rho(z=0)\rangle_{xy}}c_{\rm s}$. In the same units $B^0_{\rm eq} \approx 0.1$.

Reconnection Rate and Different Regimes

1. Sweet-Parker model (Parker (1957); Sweet (1969)):

$$V_{\rm rec} = V_{\rm A} S^{-1/2}$$

Lundquist number:

$$S = V_{\rm A} L/\eta$$

2. Lazarian-Vishniac (1999)

$$V_{\rm rec} \sim V_{\rm A} M_{\rm A}^2$$

Alfven Mach number:

$$M_{\rm A} = u_{\rm rms}/V_{\rm A}$$

3. Loureiro-Schekochihin-Cowley (2007)

$$V_{\rm rec} \sim 10^{-2} V_{\rm A}$$

Formation and Destruction of the Current Sheet

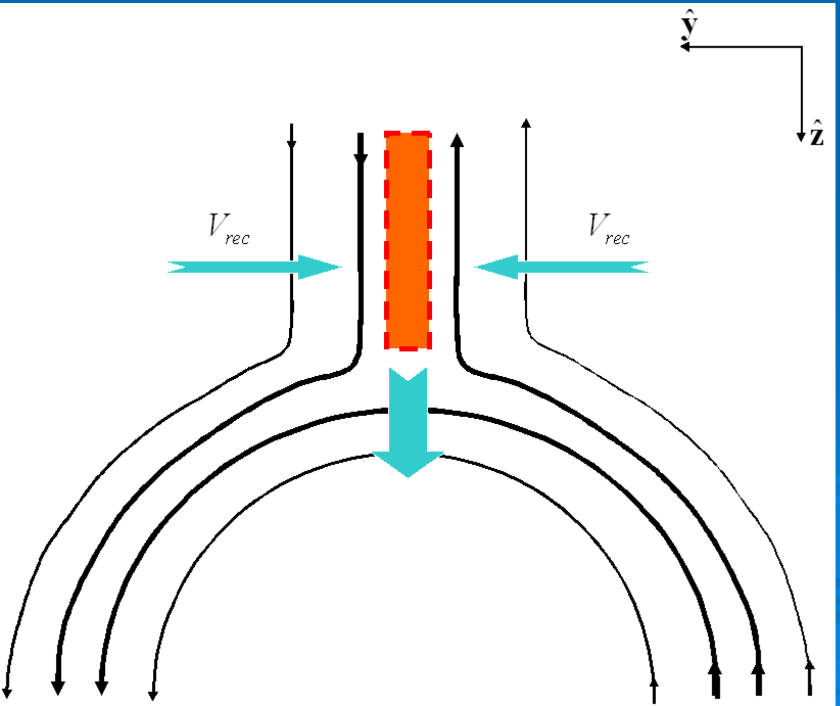

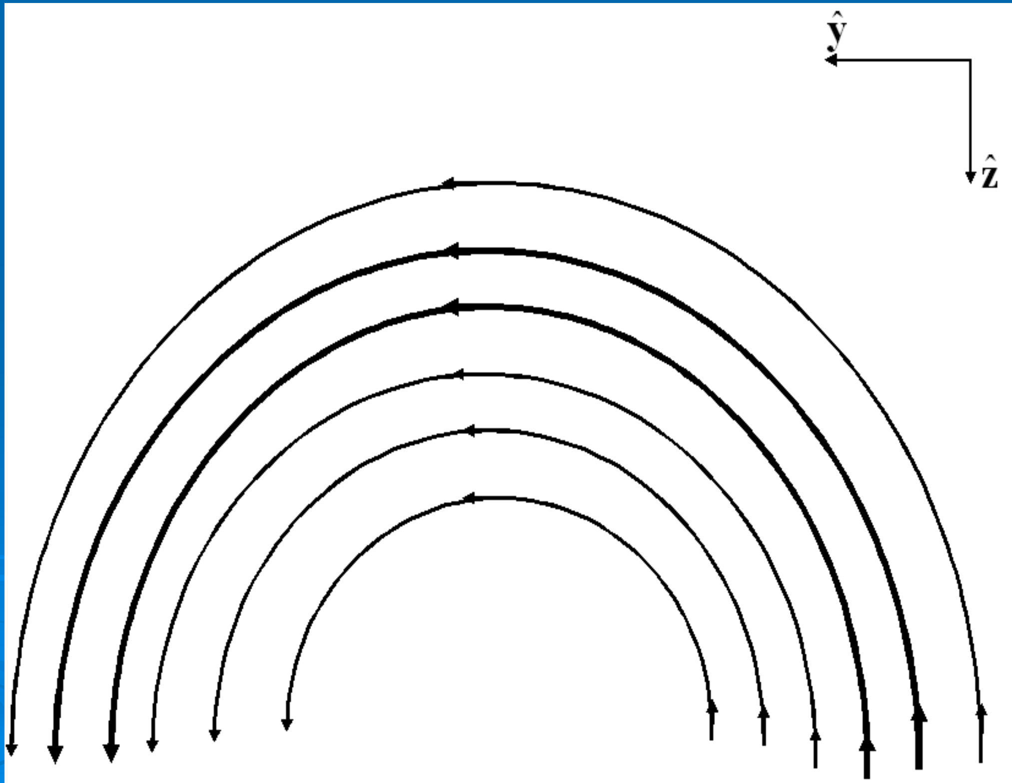

Formation of Current Sheet

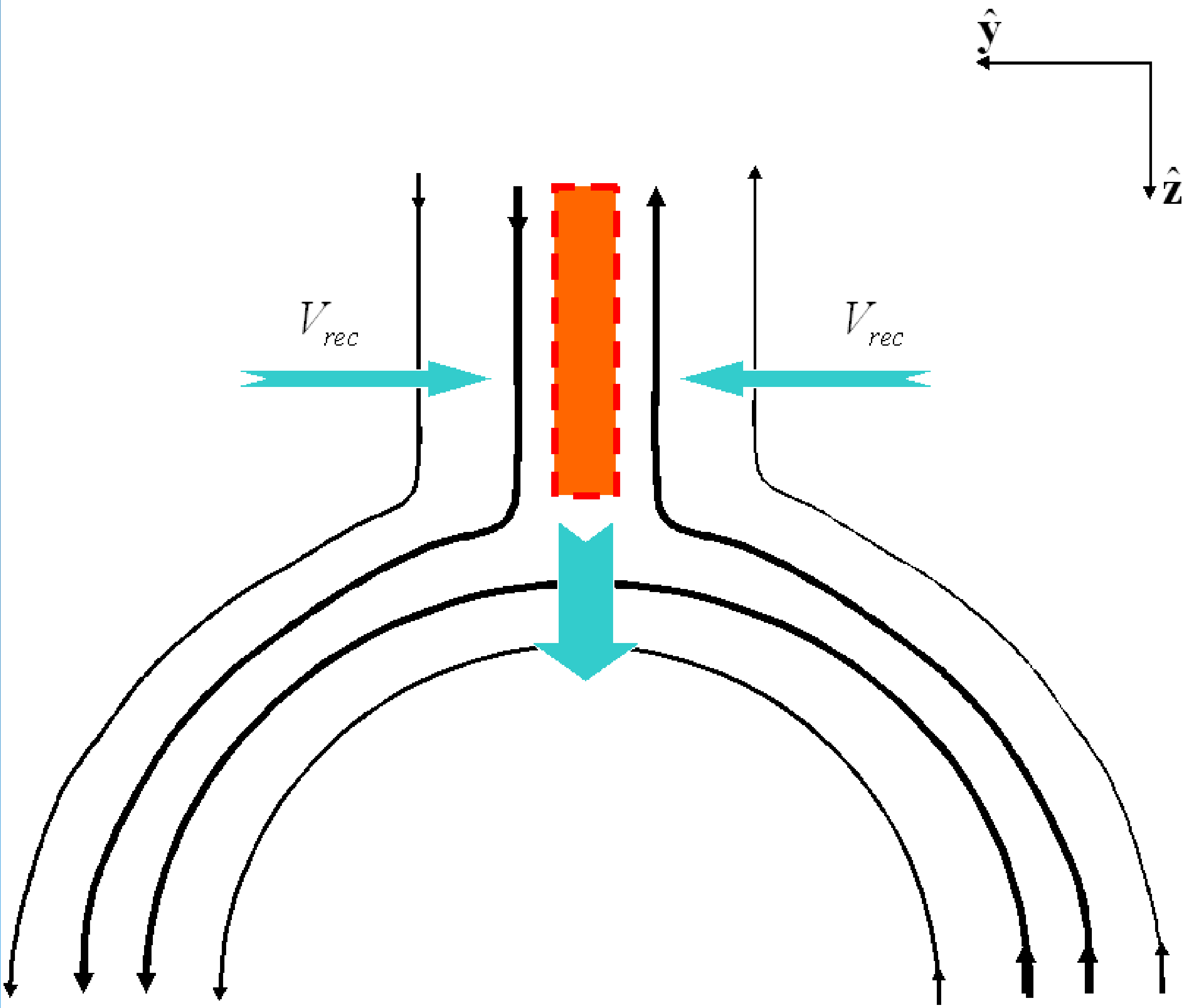

Formation of the Current Sheet and Reconnection: Rm=130

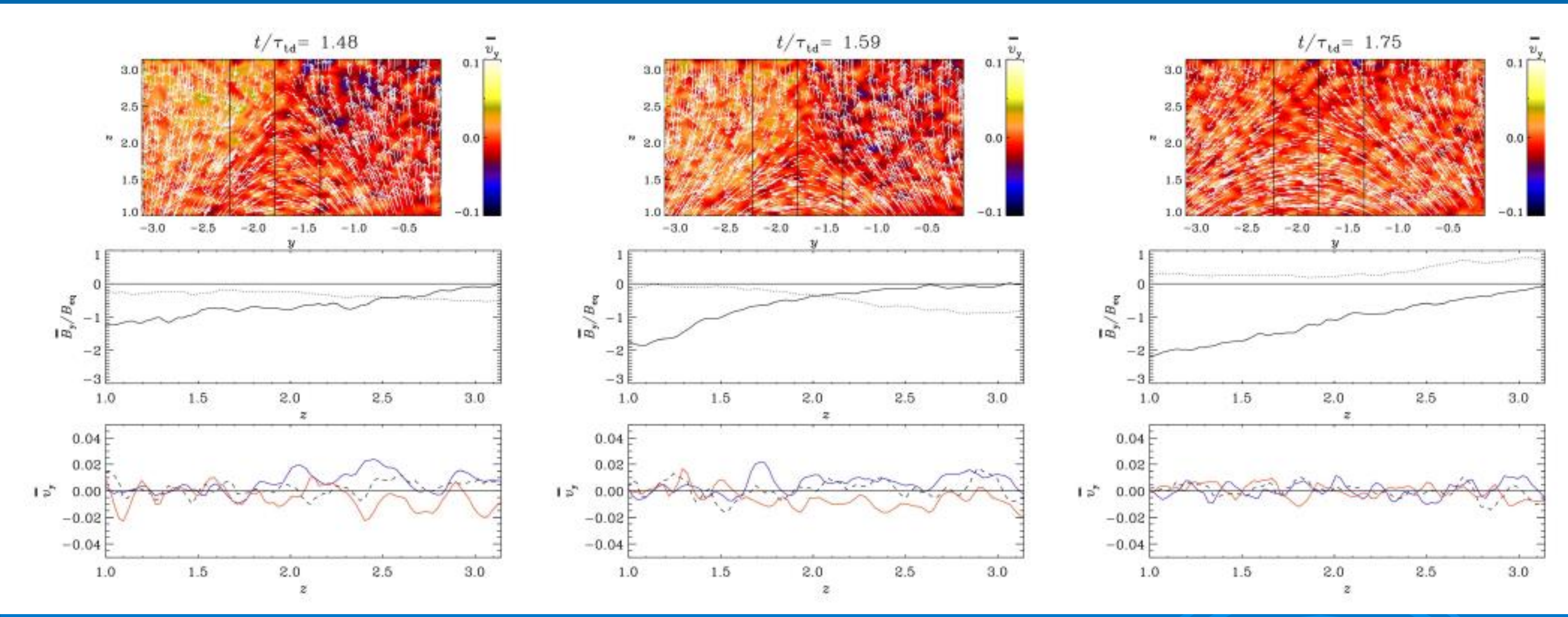

$$\mathrm{Re}_\mathrm{M} \equiv \mathrm{Re}\,\mathrm{Pr}_\mathrm{M} = u_\mathrm{rms}/\eta k_\mathrm{f}$$

Formation of the Current Sheet and Reconnection: Rm=130

$$\mathrm{Re}_M \equiv \mathrm{Re}\,\mathrm{Pr}_M = u_{\mathrm{rms}}/\eta k_{\mathrm{f}}$$

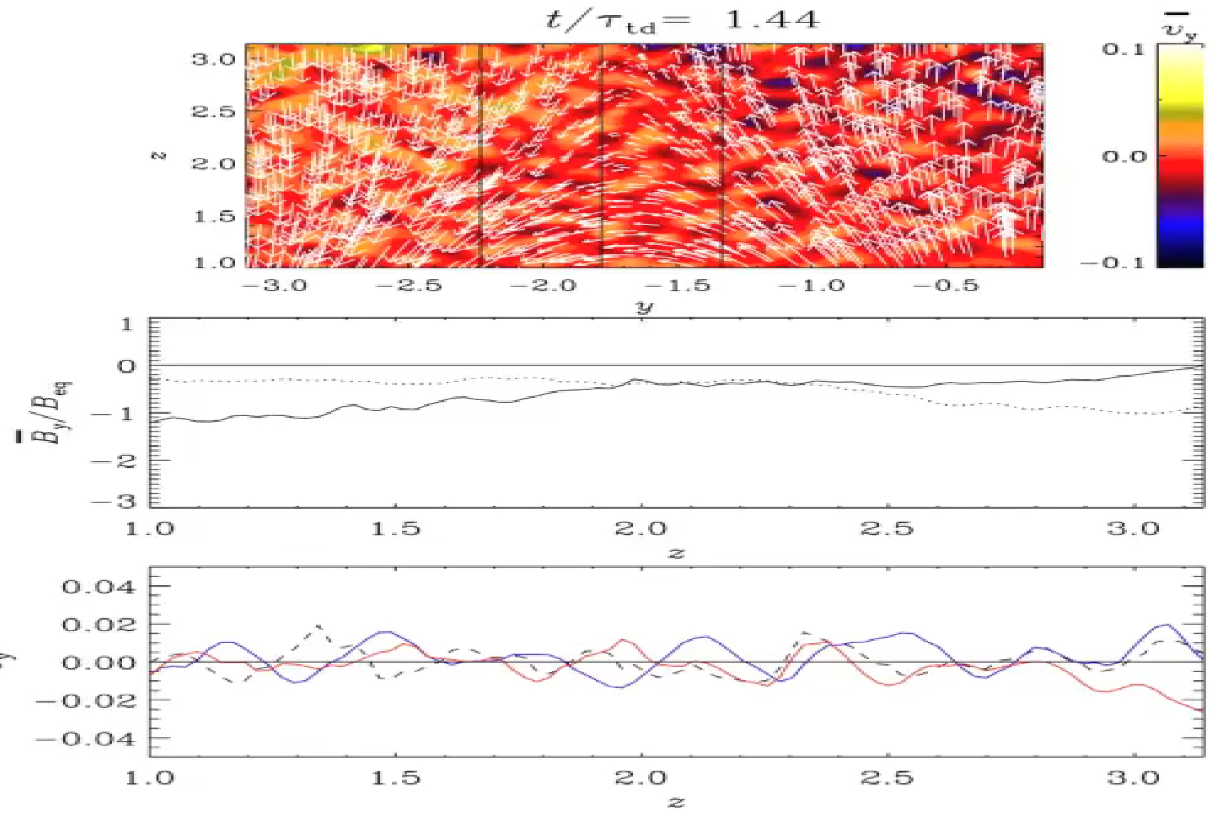

The Rate of Reconnection

The Ohm's law:

$$\eta \boldsymbol{J} = \boldsymbol{E} + \boldsymbol{U} \times \boldsymbol{B}$$

The rate of reconnection:

$$V_{\mathrm{rec}} = \frac{|\langle \boldsymbol{E} \rangle|}{|\langle \boldsymbol{B} \rangle|} = \frac{|\eta \langle \boldsymbol{J} \rangle - \langle \boldsymbol{U} \times \boldsymbol{B} \rangle|}{|\langle \boldsymbol{B} \rangle|}.$$

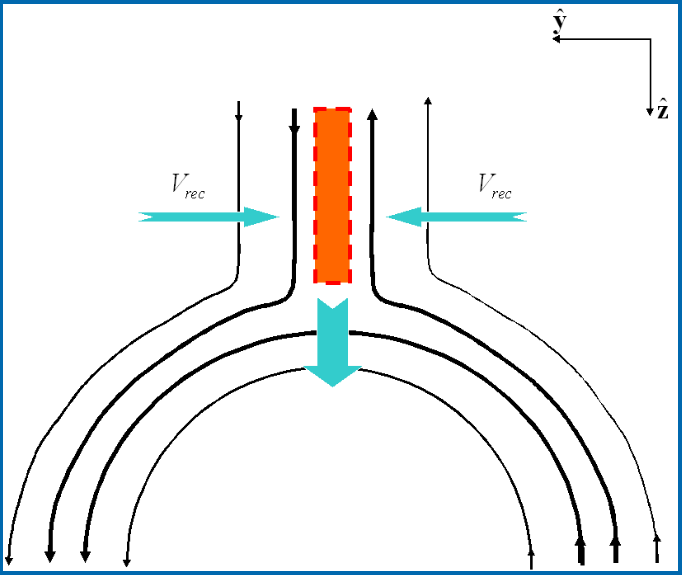

Angular brackets imply averaging along z-direction.

TABLE 2
SUMMARY OF THE RECONNECTION PARAMETERS.

Run	Re_{M}	$L_z{}^{\max}$	η	$u_{\mathrm{rms}}/c_{\mathrm{s}}$	$V_{\mathrm{rec}}/c_{\mathrm{s}}$	$V_{\mathrm{A}}/c_{\mathrm{s}}$	M_{A}	S	$S^{-1/2}$	$V_{\mathrm{rec}}/V_{\mathrm{A}}$	$\mathrm{M}_{\mathrm{A}}^2$
D1	16	0.69	2×10^{-4}	0.09	0.007	0.12	0.75	414	0.049	0.058	0.56
RM1	50	0.75	5.7×10^{-5}	0.086	0.007	0.3	0.4	3947	0.016	0.023	0.16
RM2	130	0.81	2×10^{-5}	0.078	0.007	0.48	0.16	19440	0.007	0.014	0.026

$$\mathrm{Re}_{\mathrm{M}} \equiv \mathrm{Re}\,\mathrm{Pr}_{\mathrm{M}} = u_{\mathrm{rms}}/\eta k_{\mathrm{f}}$$

Reconnection Rate and Different Regimes

1. Sweet-Parker model (Parker (1957); Sweet (1969)):

$$V_{\rm rec} = V_{\rm A} S^{-1/2}$$

Lundquist number:

$$S = V_{\rm A} L/\eta$$

2. Lazarian-Vishniac (1999)

$$V_{\rm rec} \sim V_{\rm A} M_{\rm A}^2$$

Alfven Mach number:

$$M_{\rm A} = u_{\rm rms}/V_{\rm A}$$

3. Loureiro-Schekochihin-Cowley (2007)

$$V_{\rm rec} \sim 10^{-2} V_{\rm A}$$

Formation of the Current Sheet and Reconnection: Rm=16

$$\mathrm{Re}_{\mathrm{M}} \equiv \mathrm{Re}\,\mathrm{Pr}_{\mathrm{M}} = u_{\mathrm{rms}}/\eta k_{\mathrm{f}}$$

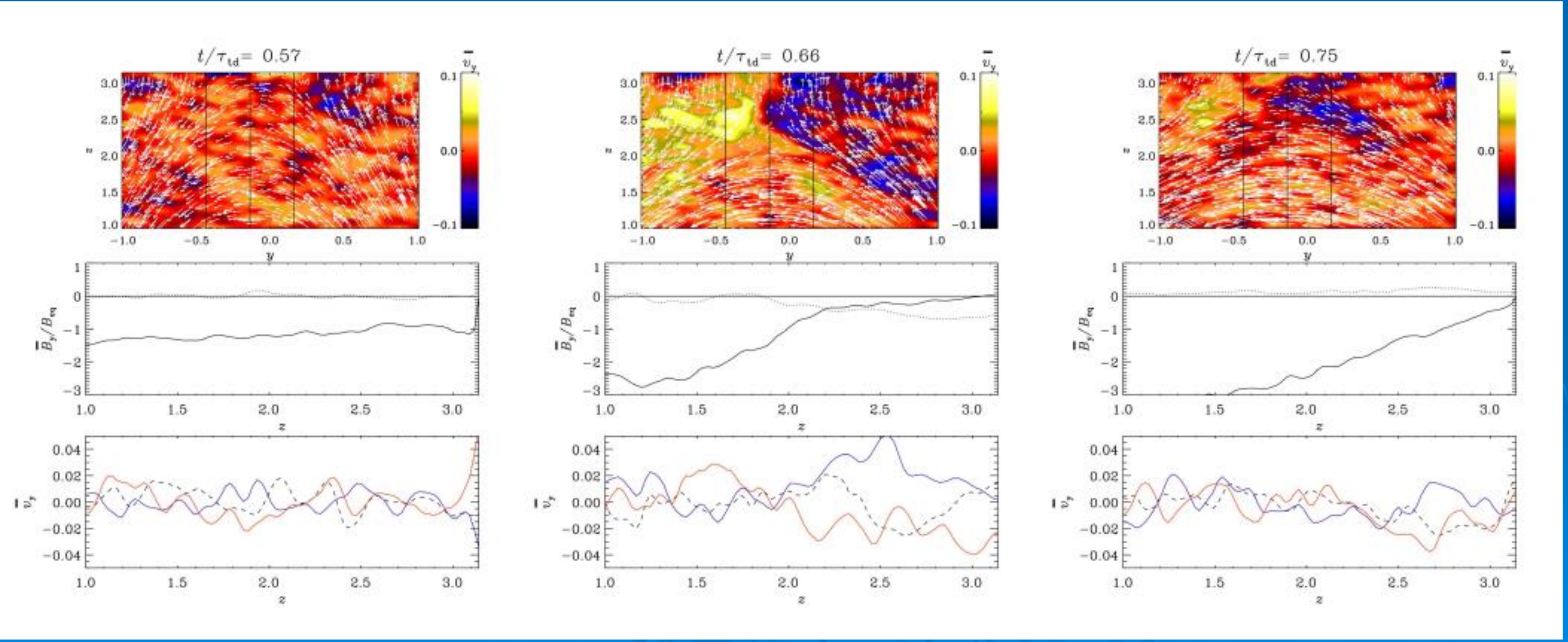

Formation of the Current Sheet and Reconnection: Rm=16

$$\mathrm{Re_M} \equiv \mathrm{Re}\,\mathrm{Pr_M} = u_{\mathrm{rms}}/\eta k_{\mathrm{f}}$$

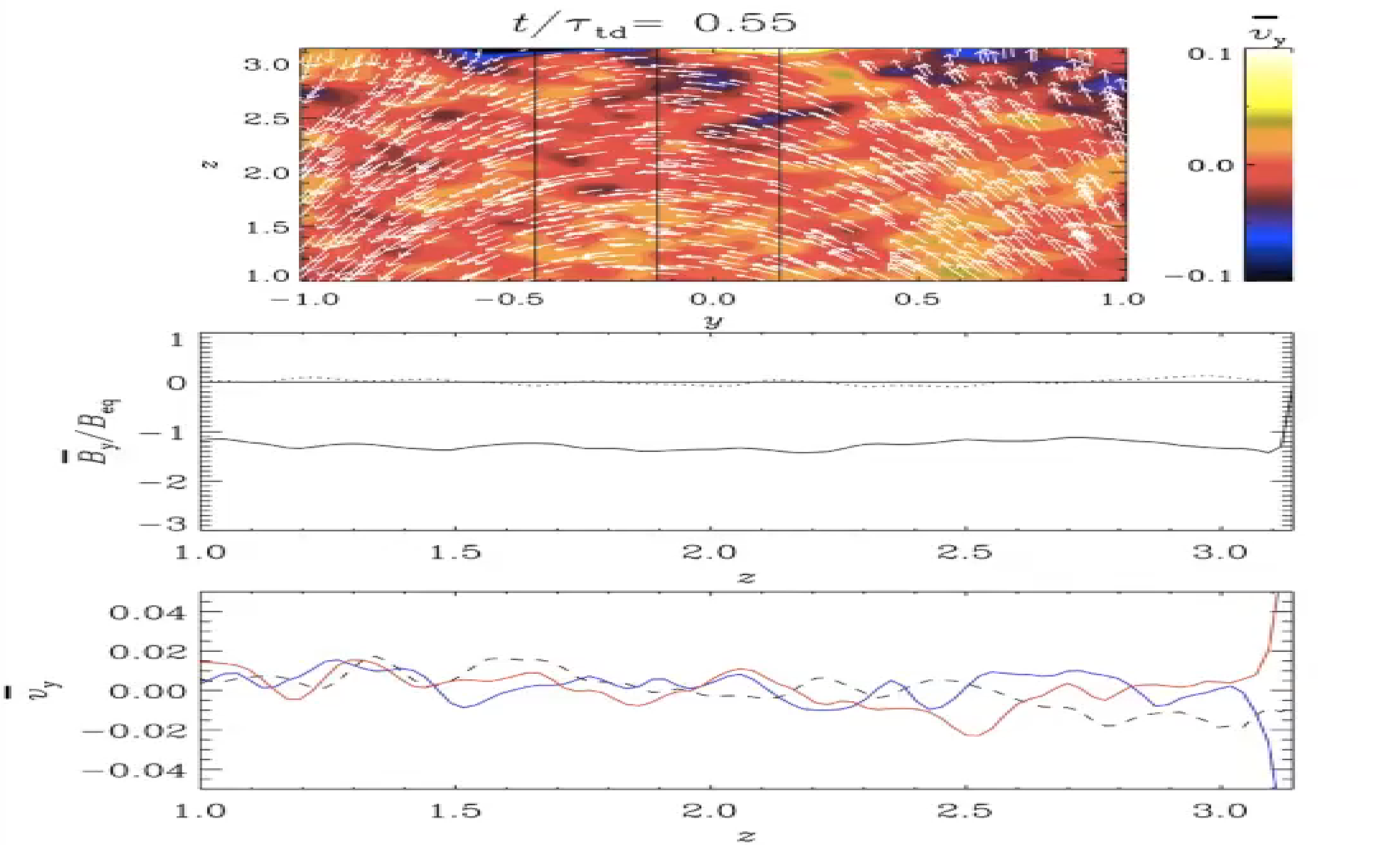

Formation of the Current Sheet and Reconnection

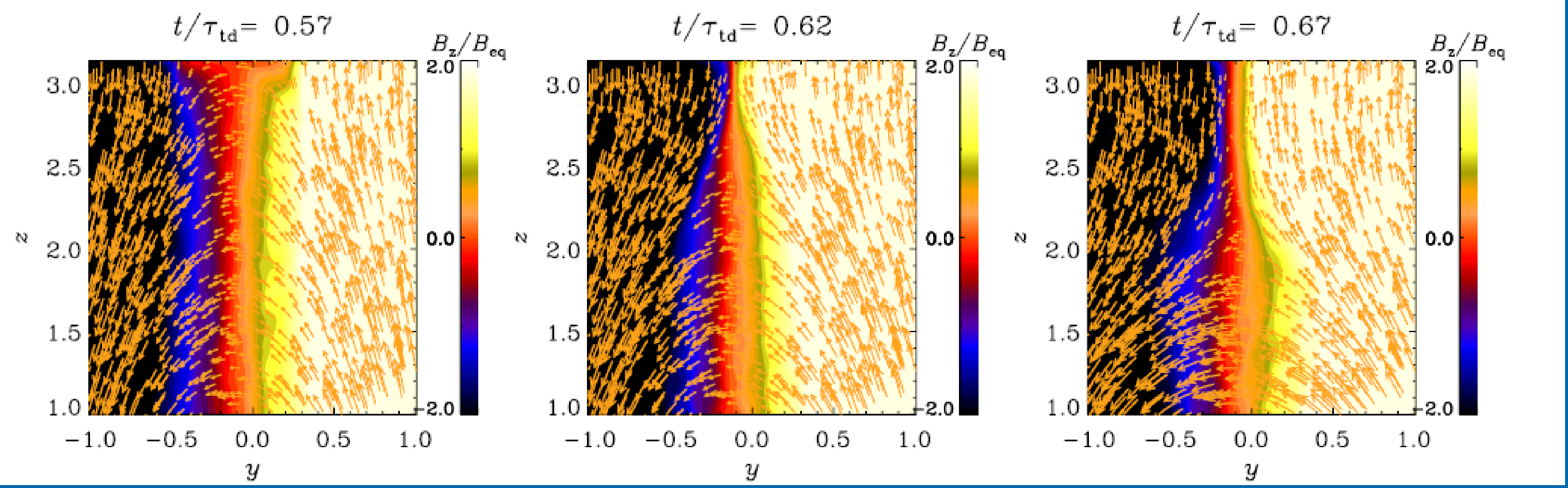

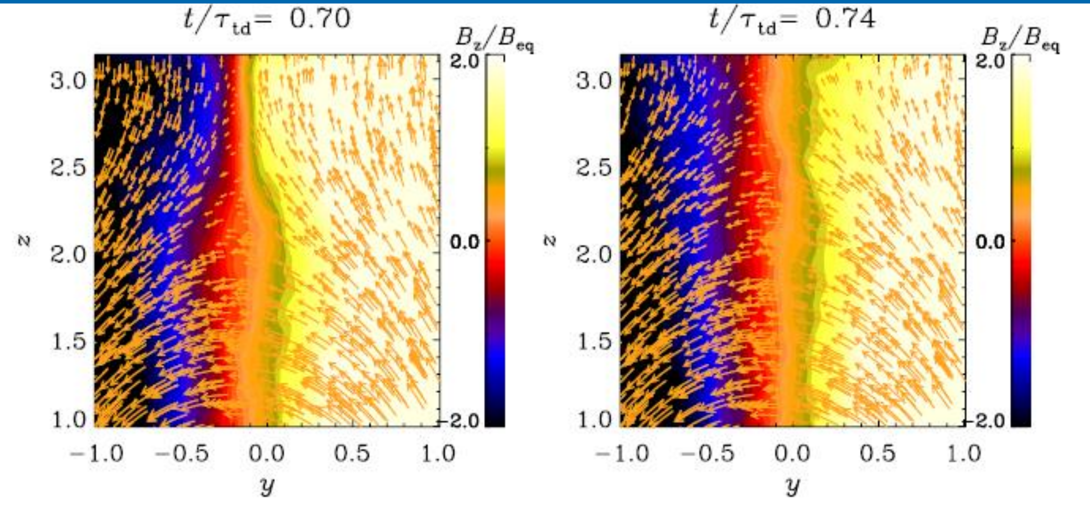

Summary

- Generation of magnetic fluctuations in a turbulence with large plasma beta results in a strong reduction of the large-scale magnetic pressure, so that effective magnetic pressure (sum of turbulent and non-turbulent contributions) can be negative.
- This causes excitation of negative effective magnetic pressure instability (NEMPI) and formation of the large-scale bipolar magnetic structures which are reminiscent Active Regions.
- DNS of two-layer systems with a helical forcing layer demonstrate formation of bipolar structures and turbulent reconnection with the rate that is independent of magnetic Reynolds number. This is the first example of turbulent reconnection in nonlinear dynamos.

THE END